PAPER

Check for updates

Measuring local pH at interfaces from molecular tumbling: A concept for designing EPR-active pH-sensitive labels and probes†

Maxim A. Voinov, [ID] Nicholas Nunn, [ID] Roshan Rana, Atli Davidsson, [ID] Alex I. Smirnov [ID] and Tatyana I. Smirnova [ID] *

Molecular probes and indicators are broadly employed for pH measurements in bulk media and at interfaces. The underlying physical principle of pH measurements of most of these probes is based on a change in the electronic structure that, for example, results in a shift of the emission peak of the fluorescence probes, changes in NMR chemical shifts due to the affected electronic shielding, or magnetic parameters of pH-sensitive nitroxides as measured by EPR. Here we explore another concept for measuring local protonation state of molecular tags based on changes in rotational dynamics of electron spin-bearing moieties that are readily detected by conventional continuous wave X-band EPR. Such changes are especially pronounced at biological interfaces, such as lipid bilayer membranes, due to the probe interactions with adjacent charges and polarizable dipoles. The concept was demonstrated by synthesizing a series of pH-sensitive nitroxides and spin-labelled phospholipids. EPR spectra of these newly synthesized nitroxides exhibit relatively small – about 0.5 G – changes in isotropic nitrogen hyperfine coupling constant upon reversible protonation. However, spin-labelled phospholipids incorporated into lipid bilayers demonstrated almost 6-fold change in rotational correlation time upon protonation, readily allowing for pK_a determination from large changes in EPR spectra. The demonstrated concept of EPR-based pH measurements leads to a broader range of potential nitroxide structures that can serve as molecular pH sensors at the desired pH range and, thus, facilitates further development of spin-labelling EPR methods to study electrostatic phenomena at chemical and biological interfaces.

Introduction

Effect of reversible protonation on EPR spectra of free radicals bearing protonatable groups was first reported in the middle of 1960s.[1–3] It was shown that the protonated and non-protonated radical species can be readily differentiated by their EPR spectra due to changes in magnetic parameters, such as isotropic nitrogen hyperfine coupling constant A_{iso} and isotropic *g*-factor g_{iso}, upon protonation. This observation suggested that EPR spectroscopy of free radicals could be employed for studying proton transfer and related phenomena in chemical and biological systems. However, practical applications of the observed effect required designing and synthesizing free radicals that, in addition to measurable changes in magnetic parameters upon protonation, would also be stable under experimental conditions. Nitroxide-type free radicals are good candidates for such applications. Indeed, some of these nitrox-

ides have been shown to undergo reversible protonation at the oxygen atom of the N–O• moiety in concentrated acids or non-aqueous solutions without the loss of the paramagnetism.[4–6] However, in strongly acidic aqueous solutions most of the nitroxides undergo disproportionation to form EPR-silent oxoammonium salt and hydroxylamine[7,8] making them unsuitable for experiments in aqueous media. Years later it was discovered that in some nitroxides, and particularly those bearing strongly basic groups, a positive charge resulting from protonation of these groups makes the consecutive protonation of a weakly basic N–O• moiety, and, hence, disproportionation, much less favourable. This finding paved the way to design and application of such nitroxides as EPR active pH probes in physicochemical and biophysical studies. For example, 4-amino derivatives of the 2,2,6,6-tetramethylpiperidine nitroxide Tempo were employed for measuring pH gradients across membranes based on the differences in membrane-binding properties of protonated and non-protonated nitroxide species.[9,10] However, small effects of protonation on magnetic parameters of the EPR spectra in such nitroxides ($\Delta A_{iso} = 0.13$ G,[11] the difference between A_{iso} of the non-protonated, R•, and protonated, R•H+, forms of the nitroxide) severely limited their

Department of Chemistry, North Carolina State University, 2620 Yarbrough Drive, Raleigh, NC 27695, USA. E-mail: tismirno@ncsu.edy

†Electronic supplementary information (ESI) available. See DOI: https://doi.org/10.1039/d4ob00167b

3652 | *Org. Biomol. Chem.*, 2024, **22**, 3652–3667

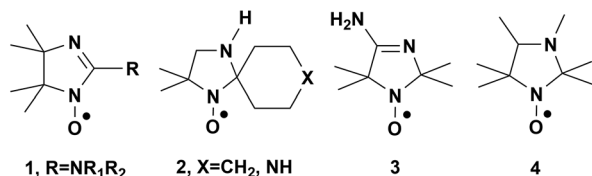This journal is © The Royal Society of Chemistry 2024

Fig. 1 pH-Sensitive 2-imidazoline, 3-imidazoline and 1,3-imidazolidine nitroxides.

practical application as EPR pH probes. Nitroxides of the 2-imidazoline series **1** (Fig. 1) show pH-induced spectral changes in physiological pH range and a relatively large – up to $\Delta A_{N1} \approx 2.40$ G and $\Delta A_{N3} \approx 1.40$ G – difference in the nitrogen hyperfine coupling constants of the protonated and non-protonated forms.[12] Unfortunately, the EPR spectra of these nitroxides are rather complex due to hyperfine couplings to three non-equivalent nitrogen atoms. This complicates analysis of protonation phenomena.

Broad applications of protonatable nitroxides in biophysical studies became possible only in the early eighties after two groups of researchers independently discovered the effect of pH on EPR spectra of imidazolidine nitroxides **2** and **4** and 3-imidazoline **3** (Fig. 1).[13,14] For these nitroxides the difference between $A_{iso}R^{\bullet}$ and $A_{iso}R^{\bullet}H^{+}$ was found to be $\Delta A_N \approx 1.0$ G. Such a large value of ΔA_N simplified analysis of the nitroxide protonation phenomena from fast motion EPR spectra consisting of three sharp, equally spaced, hyperfine lines arising from hyperfine coupling to ^{14}N nucleus. Since then, a significant progress was made in both synthesis of pH-sensitive nitroxide spin labels and probes and also development of associated EPR methods for studies of proton transfer and local electrostatic phenomena in a broad range of biological and chemical systems (for reviews see ref. 11 and 15–17).

Today, pH-sensitive EPR probes are finding numerous applications for monitoring local pH in biomedical studies. pH regulation is critical for a myriad of physiological functions like cellular metabolism, blood pH regulation, and a function of the digestive system where a disruption of pH balance is linked to various pathological conditions.[18] Despite a significant decay of the EPR signal intensity in biological environment, nitroxides in conjunction with low-frequency EPR spectroscopy and imaging techniques have been shown to enable reproducible and accurate noninvasive pH determination *in vitro* and *in vivo*.[19–21] The use of pH-sensitive nitroxides in low-field EPR spectroscopy and imaging is based exclusively on the difference in hyperfine constants between protonated and non-protonated forms and has been shown to provide high-precision measurements of pH[19,22–24] with accuracy as high as 0.1 pH units.[23,25]

Nitroxide probes with low pK_a values have been used for monitoring acidic pH in the stomach of rodents in experiments *in vivo* and to follow such changes upon administration of different antacid medications.[20,26–28] The use of EPR in tissue with pH homeostasis close to neutral, such as tumor tissues, was enabled by designing probes with higher pK_a

values, extended half-life *in vivo*, and by modification of membrane permeability of probes to ensure an extracellular localization.[29–31] Such probes have been applied to studies of tumor tissue acidosis in live mice by enabling quantitative visualization of regional changes in extracellular pH associated with altered tumor metabolism.[29,32] More recently, such probes were shown to be able to detect an increased extracellular acidification in tumor tissue following treatment of an animal with a metabolism targeting inhibitor.[33] Recently, development of pH-sensitive EPR probes moved beyond nitroxide compounds with syntheses of new dual-function trityl radicals capable to report on both pH and O_2 concentration in tumor tissues.[34–37]

pH-Sensitive nitroxides are also finding applications in other fields, such as materials and nanoscience. For example, measurements of pK_a of pH-sensitive nitroxides were utilized to evaluate acidic and electrostatic properties of porous materials like mesoporous molecular sieves,[38,39] Xerogels,[40] nanoporous anodic aluminum oxide (AAO),[41] and silica nanoparticles-water interfaces.[42]

Without risking to move too far off course of the study, we also would like to mention an increased interest in use of pH-sensitive EPR-active compounds as smart control agents in chemical synthesis.[43] For example, pH-switchable alkoxyamines have been used to control the polymerization of styrene and butyl acrylate[44] and the protonation state of the nitroxide has been shown to influence rates of nitroxide-mediated polymerization (NMP).[45–47]

As illustrated above, continued synthetic efforts over the last two decades yielded a selection of pH-sensitive probes and labels covering a broad pH range. However, analysis of the literature data shows that most if not all pH-sensitive nitroxides synthesized to this date are based on modifications of the same two core structures – 3-imidazoline **3** and 1,3-imidazolidine **4** (Fig. 1). Undoubtedly, there is an explanation for that: the protonatable amidino and tertiary amino functionalities in the structures of 3-imidazoline **3** and 1,3-imidazolidine **4** heterocycles, respectively, are located two σ-bonds away from the EPR-active N–O$^{\bullet}$. Such design is close to the optimal one based on several considerations. Firstly, the locations of the protonatable functionalities close to the spin-bearing N–O$^{\bullet}$ moiety cause rather significant ΔA_N shifts of ~0.8–1.4 G upon the change in the protonation state of the basic groups. The change in A_{iso} of about 1 G simplifies accurate quantification of the individual components of EPR spectra corresponding to the protonated or non-protonated forms of the nitroxide, especially when the spin probe/label tumbling rate falls into the fast motion regime. Moving the protonatable functionality further away from the N–O$^{\bullet}$ group significantly reduces the ΔA_N value (for example, 4-amino-2,2,6,6-tetramethylpiperidine 1-oxyl was found to have ΔA_N of only ≈ 0.13 G (ref. 11)) and, as a result, lowers the accuracy of the pK_a determination. We note here that the accuracy of the ΔA_N measurement can be significantly improved by using least-squares simulation of EPR spectra (for a description of fitting software see,[48–51] for practical applications, see ref. 52 and 53). Secondly, an electron-

This journal is © The Royal Society of Chemistry 2024

Org. Biomol. Chem., 2024, **22**, 3652–3667 | **3653**

withdrawing effect of the N–O• group at this distance from the protonatable moiety remains to be moderate so the pK_a values of probes would fall within the practically useful pK_a range (*i.e.*, 3÷8 units of pH). Note that the strong electron withdrawing effect of the N–O• group causes a reduction of the intrinsic pK_a's of basic functionalities by several units of pK_a.[14,54] If the protonatable group is located to the N–O• moiety closer than in **3** or **4**, the pK_a of the probe will be too low for practical applications. Taken together, these two factors significantly limit available options in designing new EPR pH probes with desirable properties, such as pK_a range, partitioning coefficients between polar and apolar phases, probe binding affinities, *etc.*, that can be tailored to specific applications.

Previously, we introduced phospholipids covalently modified with pH-sensitive nitroxides at the head group as EPR spin probes for studying interfacial electrostatic phenomena in detergent micelles and lipid bilayers.[55–57] In such systems these lipid-based probes position the pH-sensitive nitroxide group at the aqueous side of the interfacial region while the lipid tail is inserted into the lipid phase. For lipid bilayers above and below the main phase transition temperature, the probes demonstrated pH-dependent X-band (9.5 GHz) EPR spectra that fall into intermediate or slow-motion regime in both protonated and non-protonated forms. When recorded at intermediate pH values, the spectra of protonated and non-protonated forms of the nitroxides were not fully resolved as in the fast motion limit; however, the changes in the EPR line shapes were significant to allow for accurate determination of a fraction of protonated nitroxide from least-squares simulations assuming a slow-exchange two-component model.[55–57] It should be noted here that the changes in EPR line shapes in such systems are primarily caused by a reduction of the tumbling rate of the nitroxide upon protonation rather than effects of the nitroxide protonation state on its magnetic parameters. Indeed, the maximum reported change in the isotropic nitrogen hyperfine coupling constant A_{iso} upon protonation of nitroxides of $\Delta A_{iso} = 1.35$ G (ref. 11) is significantly smaller than the typical X-band peak-to-peak line widths – about 5 G or more – of the individual spectral components of spin-labelled phospholipids embedded into a lipid bilayer. Such large line-widths make the observations of the nitroxide protonation through changes in magnetic parameters practically impossible. However, significant changes in EPR line shapes arising from a more restricted rotation of the probe are still observed. These changes in rotational dynamics are attributed to electrostatic interactions of a charged (protonated) form of the nitroxide with a charged bilayer interface and/or a change in the effective hydrodynamic radius/hydrogen bonding network of the probe resulting from protonation. The latter effect was previously observed in electrically neutral Triton X-100 micelles.[55–57] Thus, one can hypothesize that the nitroxides with the ionizable functionality located sufficiently far from the N–O• group to exert a minimal or no effect at all on A_{iso} could still serve as EPR pH probes in sterically restricting environments, such as lipid bilayers, detergent micelles, or lipid–protein interface, as long as the tumbling of the charged

and the neutral forms differs significantly. Proving this hypothesis would provide synthetic chemists with more freedom in the challenging task of designing pH-sensitive nitroxide probes and, as a result, significantly expand the arsenal of pH-sensitive probes for biophysical and physicochemical EPR studies.

We note here that back in 1974 Barratt and Laggner observed pH effects on EPR line shapes of spin-labelled fatty acids incorporated into lecithin multilamellar vesicles (MLVs).[58] The authors explained the effect by an increase in anisotropy of molecular tumbling arising from about 6 Å dislocation of the probe along the membrane normal upon an ionization of the probe carboxylic group remote to the nitroxide.[58] Such repartitioning probes were then used to investigate surface electrostatic properties of lipid bilayers and lipid–protein interactions by analysing the fractions and rotational dynamics of multicomponent EPR spectra of spin-labelled steric acids arising upon ionization of the carboxylic group.[59–61] A method of determination of the membrane potential from partitioning of small nitroxides between aqueous and lipid phases resulting in different EPR spectra due to changes in molecular tumbling was also developed.[62]

The general approach to pH determination from EPR spectra described here does not require any probe repartitioning as it based on a universal observation that diffusion of a charged molecular probe is slowed down by the counterions that have to move together with the probe.[63] This effect is magnified at interfaces where other charges or dipoles are present and where nitroxide X-band EPR spectra of membrane probes fall into an intermediate motion regime making the spectra very sensitive to small changes in the rotational correlation time. Thus, in this proof-of-concept study we focused on the synthesis and an initial EPR characterization of pH-sensitive nitroxide spin labels and spin-labelled phospholipids designed within this new concept – to report on their ionization state through changes in the rotational dynamics observed by EPR. Spin labels were characterized by X-band EPR in aqueous solutions, whereas spin-labelled phospholipids were titrated in model multilamellar vesicles composed of either 1-palmitoyl-2-oleoyl-*sn*-glycero-3-phospho-(1′-*rac*-glycerol) (POPG) or 1-palmitoyl-2-oleoyl-*sn*-glycero-3-phosphocholine (POPC). Also, we demonstrate that EPR-active pH-sensitive phospholipids can be synthesized in one step directly from the parent phosphatidylethanolamine (PE) lipid *via* a reductive amination reaction of the proper nitroxide containing either ketone or aldehyde group.

Results and discussion

Synthesis

Thiol-methanethiosulfonate click reaction was chosen as the leading method for covalent modification of the lipid polar head group with pH-sensitive spin label(s). This choice was justified by many years of successful application of this click chemistry in site-directed spin labelling (SDSL) EPR studies,[64]

3654 | *Org. Biomol. Chem.*, 2024, **22**, 3652–3667

This journal is © The Royal Society of Chemistry 2024

superior selectivity of this reaction with respect to SH-group, commercial availability of a headgroup thiol-modified phospholipid 1,2-dipalmitoyl-sn-glycero-3-phosphothioethanol, and also by our previous experience in using this reaction in the protein spin labelling and the synthesis of spin-labelled phospholipids.[55–57,65] Dimethylamino-substituted pyrrolidine nitroxide **10** was used as a core molecular structure. A synthetic route to the target spin label **12** is shown in Scheme 1.

The initial compound amino acid **5** (POAC) was synthesized according to literature procedures.[66,67] Boc-protection of the primary amino group, followed by preparation of the mixed anhydride **7** and its reduction with NaBH$_4$, afforded the N-Boc-protected amino alcohol **8**. Deprotection of the latter in a boiling water–methanol (6 : 1 v/v) mixture[68] gave the amino alcohol **9** in good yield. Alkylation of the primary amino group of **9** was carried out using the Eschweiler–Clarke reaction to give the tertiary amine **10**; hydroxyl group of the latter was activated through formation of the corresponding mesylate **11**. Nucleophilic substitution of the OSO$_2$CH$_3$ group in **11** with bromide, iodide, or azide afforded corresponding derivatives **13**, **14**, and **15** (Scheme 2). Strain-promoted azide–alkyne cycloaddition of **15** with 3-amino-1-(11,12-didehydrodibenzo[b,f]azocin-5(6H)-yl)propan-1-one (DBCO-amine) readily afforded triazole adduct **16**, most likely as a mixture of syn- and anti-isomers[69,70] (Scheme 2). However, attempts to obtain the methanethiosulfonyl derivative **12** from **11** have failed.
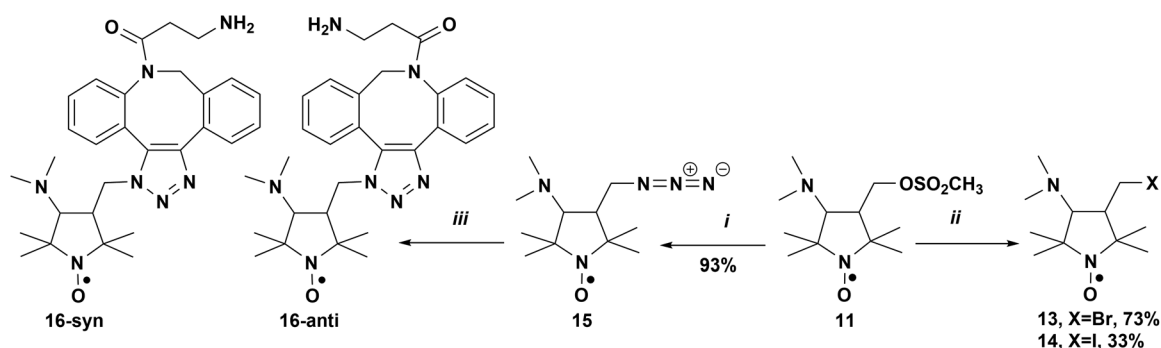
Reaction of the latter with sodium methanethiosulfonate did not afford thiosulfonate nitroxide **12**. At room temperature **11** did not react with NaSSO$_2$CH$_3$ both in DMSO and EtOH; at the elevated temperature (70 °C), an inseparable mixture of products has formed. We speculate that thiosulfonate anion might be too "soft", compared to Br$^-$, I$^-$, and N$_3^-$, to attack the "hard" electrophilic carbon adjacent to the mesylate group. Besides, the geminal methyl groups in position 2 of the pyrrolidine heterocycle could create an unfavourable steric environment for the attack by a relatively bulky methanethiosulfonate. Attempts to obtain **12** through the reaction of NaSSO$_2$CH$_3$ with halogen derivatives **13** and **14** were also unsuccessful.

To make the steric requirements for the nucleophilic substitution less demanding, a handle between the pyrrolidine heterocycle and the leaving group was introduced. This was accomplished by reacting the hydroxymethyl derivative **10** with either 2-bromoethyl isocyanate or 2-(2-bromoethoxy)tetrahydro-2H-pyran (Scheme 3). Tetrahydropyranyl protecting group in **17** was removed with aqueous acetic acid;[71] the resulting hydroxyethyl derivative **18** was converted to the mesylate **19**. Reactions of **19** and the bromo derivative **21** with NaSSO$_2$CH$_3$ afforded the methanethiosulfonate spin labels **20** and **22**, respectively.
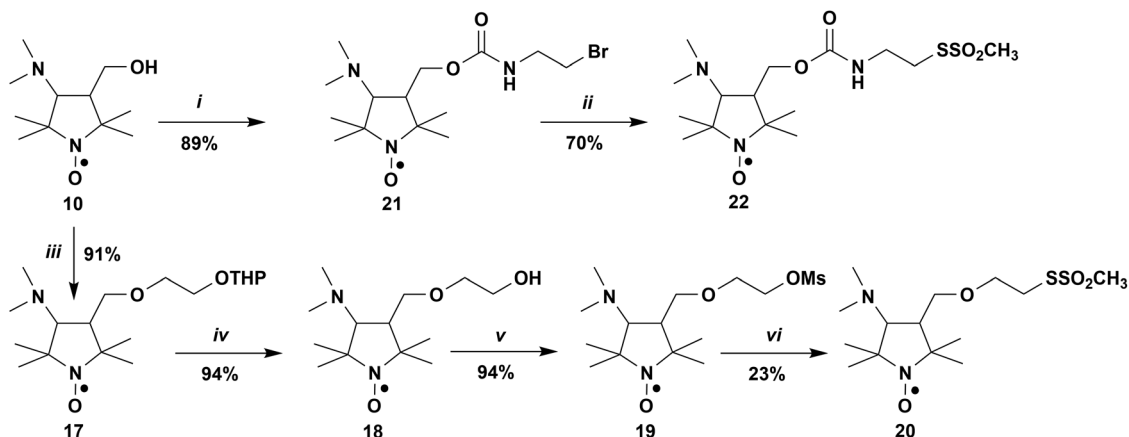
Spin-labelled phospholipids **20-PTE** and **22-PTE** (Fig. 2) were synthesized through the thiol-methanethiosulfonate click reac-
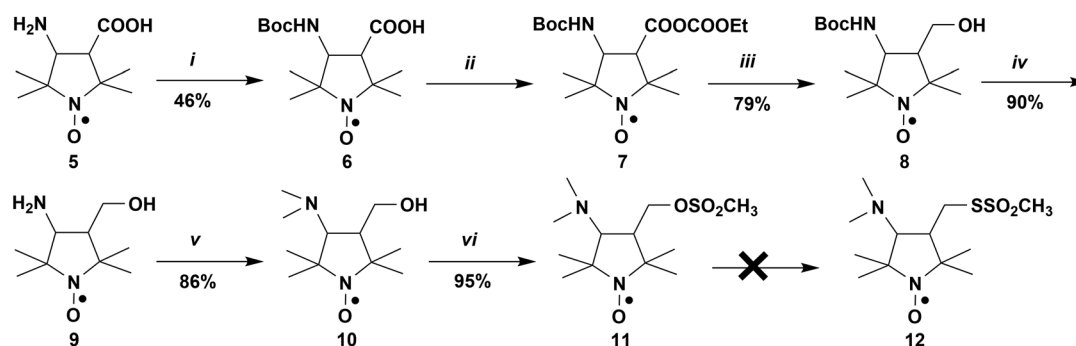
Scheme 1 (i) Di-tert-butyl dicarbonate, Et$_3$N, CH$_3$CN; (ii) ClCOOEt, Et$_3$N, ether, −10 °C; (iii) NaBH$_4$, EtOH, −15 °C; (iv) H$_2$O/CH$_3$OH, 6 : 1 v/v, reflux; (v) HCOH, HCOOH, 60 °C; (vi) Et$_3$N, CH$_3$SO$_2$Cl, CH$_2$Cl$_2$, −10 °C.

Scheme 2 (i) NaN$_3$, DMSO, 70 °C; (ii) LiBr (or LiI), DMSO, 70 °C; (iii) DBCO-amine.

This journal is © The Royal Society of Chemistry 2024

Org. Biomol. Chem., 2024, **22**, 3652–3667 | **3655**

Scheme 3 (i) Br(CH$_2$)$_2$NCO, EtOAc; (ii) NaSSO$_2$CH$_3$, DMSO, rt; (iii) Br(CH$_2$)$_2$OTHP, KOH, DMSO, rt; (iv) CH$_3$COOH–H$_2$O mixture (4 : 1 v/v), 50–55 °C, 3 h; (v) CH$_3$SO$_2$Cl, Et$_3$N, CH$_2$Cl$_2$, −10 °C; (vi) NaSSO$_2$CH$_3$, DMSO, 70 °C.
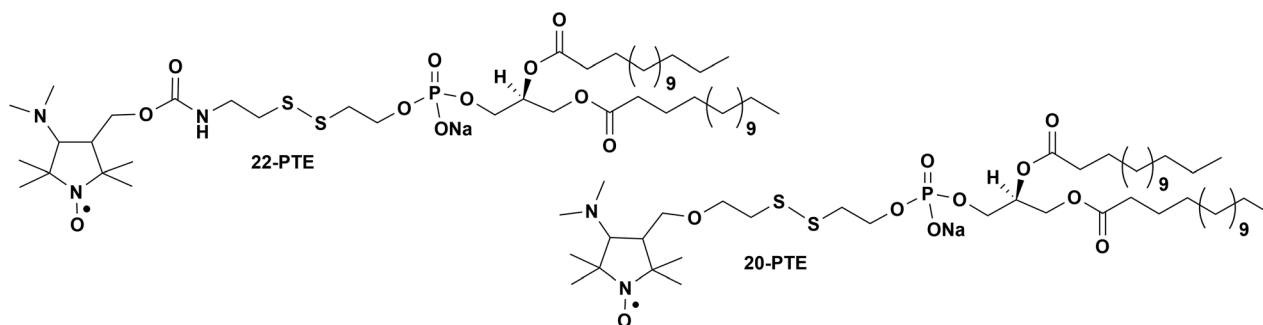

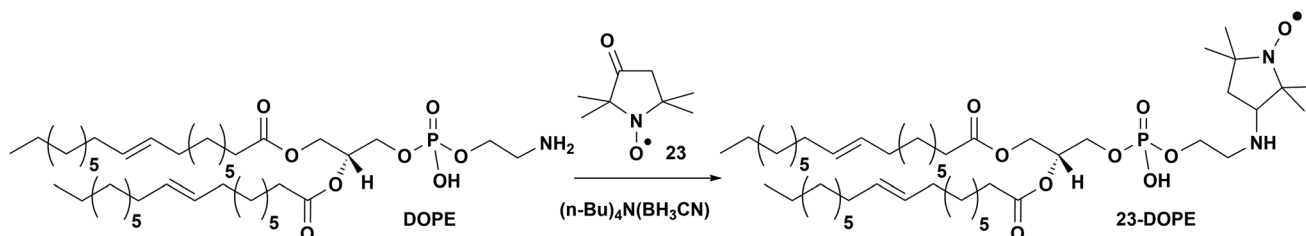**Fig. 2** Chemical structures of spin-labelled phospholipids.

tion of **20** and **22**, respectively, with a thiol-modified phospholipid 1,2-dipalmitoyl-*sn*-glycero-3-phosphothioethanol (PTE).

pH-Sensitive spin-labelled phospholipid **23-DOPE** was synthesized using a different approach – through a reductive amination of the ketone nitroxide **23**[72] with 1,2-dioleoyl-*sn*-glycero-3-phosphoethanolamine (DOPE) lipid (Scheme 4). This spin-labelling methodology presents a rather advantageous way to designing pH-sensitive EPR-active phospholipids from PE lipids because the amino functionality of the phosphoethanolamine residue becomes the protonatable group of the pH-sensitive spin-labelled phospholipid. We speculate that this methodology could also be applied for spin-labelling of protein lysine residues.

EPR characterization of novel nitroxides

Nitroxides and spin-labelled phospholipids were EPR titrated (X-band, 9.5 GHz) in aqueous solutions or lipid suspensions, respectively, to determine their pK_a's. Thiosulfonate group is known to be hydrolytically labile at basic pH[73] and pK_a of the spin label is expected to change after a covalent attachment to a molecule of interest. For these reasons, spin labels **22** and **20** were titrated in the forms of adducts with 2-mercaptoethanol **24** and **25**, respectively (Fig. 3).

The side chain structures in these adducts (Fig. 3) are similar to those of spin labels attached to the thiol group of the PTE lipid (Fig. 2), and, as we have previously reported,[55–57]

Scheme 4 Synthesis of the spin-labelled phospholipid *via* a reductive amination reaction.
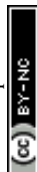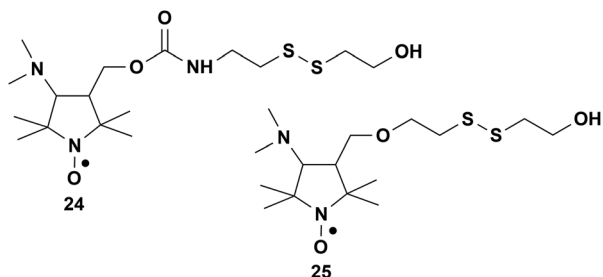
Fig. 3 Chemical structures of 2-mercaptoethanol adducts.

the hydroxyethyl moiety of these compounds is mimicking the inductive effect of the PTE head group attachment rather well. Similarly, nitroxide **26**, synthesized *via* the reductive amination of the ketone nitroxide **23** with 2-aminoethanol (Scheme 5), was used as a water-soluble model of the spin-labelled phospholipid **23-DOPE** for EPR characterization in aqueous solutions. Azide **15** was EPR-characterized both as such, and also in a form of the triazole adduct with DBCO-amine **16** (Scheme 2). The DBCO derivatives are widely used in various copper-free alkyne–azide conjugation and labelling protocols,[74–76] although this type of conjugation has a limited utility in biophysical EPR studies because of the bulkiness of the linker.

For characterization of spin-labelled phospholipids in lipid bilayers, multilamellar vesicles (MLV's) composed of either POPG or POPC were doped with **20-PTE**, **22-PTE**, or **23-DOPE** at 1 mol% using experimental protocols described elsewhere.[56,57]

Aqueous solutions of all the nitroxides synthesized in this work exhibit typical isotropic three-line X-band (9.5 GHz) EPR spectra (ESI, S69–S76†). Unlike the X-band EPR spectra of many other pH-sensitive nitroxides, the spectra of the newly synthesized compounds did not show characteristic splitting of the high-field nitrogen hyperfine component at intermediate pH values. This splitting results from a difference in nitrogen hyperfine coupling constants of protonated and non-protonated forms of a nitroxide (typically, $\Delta A_{\text{iso}} \approx 0.80\text{–}1.30$ G)[52,53] and, is indicative of a slow, on the EPR time scale, chemical exchange. According to the previously established slow-exchange condition that relates the pK_a of the nitroxide probe and the type of the chemical exchange:[77]

$$\log\left(\frac{\kappa_1^{\text{H}^+}}{\Delta\nu}\right) < pK_a < 14 - \log\left(\frac{\kappa_1^{\text{OH}^-}}{\Delta\nu}\right), \quad (1)$$

where $\Delta\nu$ is the frequency difference between high-field components of the protonated and non-protonated forms of the nitroxide; $\kappa_1^{\text{H}^+} \approx \kappa_1^{\text{OH}^-} \approx 1 \times 10^{10}$ M^{-1} s^{-1} are the forward rate constants for the diffusion controlled protonation (R$^\bullet$ + H$^+$ ⇆ R$^\bullet$H$^+$) and deprotonation (R$^\bullet$H$^+$ + OH$^-$ ⇆ R$^\bullet$ + H$_2$O) reactions, respectively.[77]

For nitroxides **10–26** $\Delta\nu(\text{MHz}) = \left(\frac{\mu_B}{h}\right) \times \frac{g}{g_e} \times \Delta A_{\text{iso}}(\text{G}) \approx 2.8 \times 0.5$ G ≈ 1.4 MHz. Then for these nitroxides pK_a values would fall into a range $3.9 < pK_a < 10.1$, and such EPR species are expected to be in a slow chemical exchange regime. However, none of the fast motion EPR spectra of the novel nitroxides revealed a splitting in the high field nitrogen hyperfine coupling components but only some extra broadening resulting in a decrease in the peak-to-peak amplitude (ESI, S69–S76†). Some of the reasons for the absence of splitting include a lack of spectral resolution as the two $m_I = -1$ lines of $\Delta B_{\text{p-p}} \approx 1.2$ G in widths are separated by only $\Delta B \approx \Delta A_{\text{iso}} \approx 0.50$ G and/or a higher than estimated exchange rate. For example, as it was shown for pH-sensitive nitroxides of the 3-imidazoline and imidazolidine series, the R$^\bullet$ ⇆ R$^\bullet$H$^+$ exchange rate could be increased by the presence of a buffer, causing the two high-field lines to coalesce. However, replacement of 50 mM phosphate buffer with 50 mM NaCl solution did not show any effect on the shape of the high-field EPR line (see ESI, S70†). Thus, we speculate that protonation of the functionality in the side chain (*e.g.*, in nitroxides **10–26**) is less sterically inhibited compared to that of the one being a part of the heterocycle, such as in 3-imidazoline and imidazolidine nitroxides. Our speculation is supported by the existing correlation between bimolecular constant of the proton exchange reaction and the steric accessibility of the protonation site.[78]

For accurate measurements of A_{iso} the experimental spectra were modelled as single-component fast-motion nitroxide spectra. The line shape of each of the nitrogen hyperfine components was approximated by a Voigt function[48] with Gaussian and Lorentzian contributions to the linewidth and the effective isotropic hyperfine constant being adjustable parameters of the fit. Isotropic nitrogen hyperfine coupling parameters of the synthesized nitroxides and titration data are summarized in Table 1.

All pH-sensitive nitroxides demonstrate a small but readily detectable $\Delta A_{\text{iso}} \approx 0.50$ G difference between the isotropic nitrogen hyperfine coupling constants of the protonated and non-protonated forms and pK_a values in the range of ~4–7 units of pH depending on the structure of the side chain. We
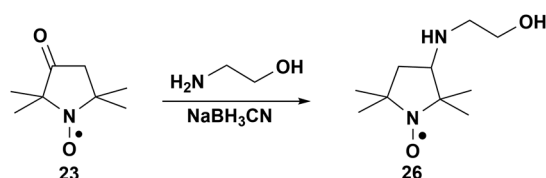
Scheme 5 Reductive amination of the ketone nitroxide **23**.

Table 1 Isotropic nitrogen hyperfine coupling constants (A_{iso}R$^\bullet$ and A_{iso}R$^\bullet$H$^+$), ΔA_{iso}, and pK_a values for aqueous solutions of selected nitroxides at 17 °C

Compound	A_{iso}R$^\bullet$, G	A_{iso}R$^\bullet$H$^+$, G	ΔA_{iso}, G	pK_a
10	15.98 ± 0.02	15.47 ± 0.02	0.51 ± 0.03	6.25 ± 0.01
15	15.78 ± 0.03	15.27 ± 0.02	0.51 ± 0.04	5.80 ± 0.02
16	15.68 ± 0.03	15.17 ± 0.03	0.51 ± 0.04	4.44 ± 0.02
18	15.97 ± 0.02	15.45 ± 0.02	0.51 ± 0.03	6.39 ± 0.01
24	15.89 ± 0.04	15.37 ± 0.05	0.52 ± 0.06	5.51 ± 0.03
25	15.95 ± 0.01	15.44 ± 0.02	0.51 ± 0.02	6.22 ± 0.06
26	16.06 ± 0.02	15.57 ± 0.01	0.49 ± 0.02	6.73 ± 0.01

This journal is © The Royal Society of Chemistry 2024

Org. Biomol. Chem., 2024, **22**, 3652–3667 | **3657**

note that adduct **16** exhibits the lowest aqueous $pK_a = 4.44 \pm 0.02$, which could be either a result of an electron-withdrawing effect of the triazole moiety, or a destabilizing electrostatic effect of the protonated 3-aminopropylamide side chain ($pK_a = 8.81 \pm 0.10$ (ref. 79)), and/or an electron-withdrawing effect of the protonated triazole moiety (triazoles have been reported to be weakly basic[80–82]), or a combination of both effects. To support EPR determination of pK_a we conducted a potentiometric titration of the compound **10**. Analysis of the potentiometric measurements (see ESI, Fig. S1†) yielded $pK_a = 6.27 \pm 0.06$, which is in good agreement with the EPR data ($pK_a = 6.25 \pm 0.01$).

To demonstrate utility of spin-labelled phospholipids **20-PTE**, **22-PTE**, and **23-DOPE** as EPR probes for biological membranes, EPR titration of these lipids in model multilamellar vesicles (MLVs) composed either of anionic phospholipid POPG or zwitterionic phospholipid POPC in fluid (17 °C) bilayer phases was performed. EPR spectra of all these spin-labelled lipids fall into an intermediate-to-slow motion regime (Fig. 4, left). It could be seen that, similar to our previous data for titration of spin-labelled lipids in model lipid bilayers,[55–57] a decrease in pH resulted in a gradual appearance of a more immobilized spectral component. We attribute the latter component to a protonated form of the nitroxide that is expected to have a slower tumbling (*vs.* uncharged nitroxide) due to electrostatic interactions with the negatively charged bilayer interface.

A clear demonstration that the protonation affects magnetic parameters of spin-labelled phospholipids such as **20-PTE** was obtained by measuring rigid limit EPR spectra at 77 K. Fig. 4 (right) compares rigid limit X-band EPR spectra of **20-PTE** in POPG MLVs at pH = 9.84 (top) when this nitroxide is expected to be in the non-protonated form with a spectrum at pH = 3.42 (bottom) when this nitroxide is fully protonated. The positions of the outer nitrogen hyperfine lines corresponding to $2A_{zz}$ of the non-protonated nitroxide are shown as dashed lines to demonstrate that this magnetic parameter is decreased upon protonation (compare top and bottom spectra in Fig. 4, right). This effect was quantified by least-squares simulation of the spectra using Pepper function of EasySpin.[83,84] The Pepper function is designed for simulations and fitting of CW EPR spectra in the absence of rotational averaging such as those observed for single crystals or the crystals grounded into a powder. Thus, this function was selected for simulating spectra obtained at 77 K.[85] The simulated spectra shown as thin lines in Fig. 4 (right) are superimposed with the experiment (thick black lines) and are nearly identical. We note that *x*- and *y*-axis principal components of both g-matrix and A-tensor of the nitroxides are typically not resolved in the rigid limit X-band EPR spectra unless the radicals are perdeuterated.[86] Thus, the main changes caused by local electric fields and hydrogen bonding are expected in A_{zz} component,[87,88] which for **20-PTE** in POPG MLVs was found to change from $A_{zz} \approx 34.34$ G to ≈ 32.84 G upon protonation. Therefore, $\Delta A_{iso} = \frac{1}{3}(\Delta A_{xx} + \Delta A_{yy} + \Delta A_{zz}) \approx \frac{1}{3}\Delta A_{zz} = 0.50 G$, which is in an excellent agreement with $\Delta A_{iso} = 0.50 \pm 0.01$ G, determined from the fast motion spectra (Table 1).

To demonstrate that the protonation of pH-sensitive nitroxides attached to the lipid polar head results in large changes in rotational tumbling, representative EPR spectra of **20-PTE** incorporated at 1 mol% into POPG MLVs and measured at 17 °C were least-squares simulated using chili function of
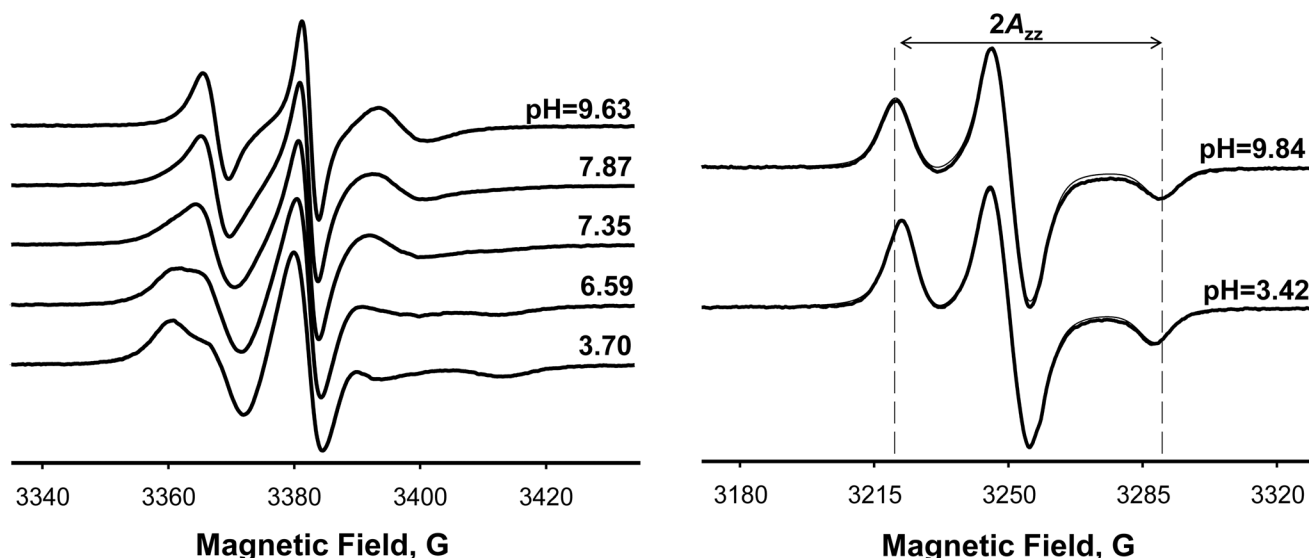

Fig. 4 Left: Representative X-band (9.5 GHz) EPR spectra from a titration of multilamellar POPG vesicles doped with 1 mol% of the spin-labelled phospholipid **20-PTE**. Spectra were measured at 17 °C. Right: Experimental rigid-limit (77 K) X-band EPR spectra from POPG MLVs doped with 1 mol% of the spin-labeled phospholipid **20-PTE** in non-protonated (top) and protonated (bottom) forms shown as thick black lines are superimposed with simulated spectra (thin black lines), which are almost indistinguishable from the experimental spectra. Approximate magnetic field positions corresponding to $2A_{zz}$ nitrogen hyperfine splitting of the non-protonated form are shown as dashed lines and pH values are indicated next to the spectra.

3658 | *Org. Biomol. Chem.*, 2024, **22**, 3652–3667

This journal is © The Royal Society of Chemistry 2024

EasySpin.[84,85] The Chili function is designed for simulations and fitting of CW-EPR spectra in the slow-motion regime, and, hence, was used for the 17 °C spectra. Simulations of EPR spectra by the Chili function is based on a solution of the Stochastic Liouville Equation (SLE). For simplicity, an isotropic rotational model was assumed, and magnetic parameters obtained from the rigid limit simulations of Fig. 4 were slightly adjusted to account for fast residual librations resulting in some pre-averaging of the anisotropic magnetic parameters. Fig. 5 shows that the best simulations (thin lines) closely follow the experimental spectra (thick lines). The spectra of non-protonated nitroxide yielded effective correlation time $\tau \approx$ 1.4 ns while rotational tumbling of the fully protonated form at pH = 3.42 demonstrated significantly longer correlation time of ≈ 8.3 ns.

Although simulations of slow-motion EPR spectra of spin-labelled lipids demonstrated a good agreement with experiment (Fig. 5), such simulations are known to be time consuming because of multiple parameters involved. Thus, in order to decrease the number of adjustable parameters and simplify the simulations, the spectra at intermediate pH values were simulated as a superposition of two components, each corresponding to the protonated and non-protonated forms of the nitroxide (*i.e.*, a slow exchange model was assumed). These two reference spectra we measured experimentally, and the weights of the individual components were adjusted during the fitting and then used to calculate a fraction $f = I_R/(I_R + I_{RH^+})$ of the non-protonated form from the corresponding double integrals of the individual components. Details of the decomposition procedure are described elsewhere.[56,57] Fig. 6 shows an example of such a two-component decomposition of an EPR spectrum of **20-PTE** in POPG MLVs. The residual of the fit – a difference between the experimental and simulated spectra – reveals only minor deviations, thus, demonstrating the applicability of the slow exchange model. To determine the pK_a of the probe, the fraction of the non-protonated form, f, was plotted as a function of pH and the experimental titration data were fitted to the Henderson–Hasselbalch equation. Fig. 7 shows such plots for titration of **22-PTE** incorporated in multilamellar vesicles composed of POPC or POPG at 17 °C, and the corresponding fits to the Henderson–Hasselbalch equation. Titration data for the three spin-labelled phospholipids incorporated in POPC or POPG multilamellar vesicles are summarized in Table 2.

Notably, unlike **22-PTE** and **23-DOPE**, the experimental titration plot for **20-PTE** in multilamellar POPC vesicles contains several reproducible outlier data points at pH below the pK_a of the probe (Fig. 8, left panel). Since this model system has no titratable groups other than tertiary amino group of the nitroxide (pK_a of the phosphate group in POPC is too low, pK_a ≈ 1.0 (ref. 89)), we ruled out a possibility of the second pK_a transition. Furthermore, when EPR titration of **20-PTE** was conducted in 200 nm unilamellar POPC vesicles (ULVs), the titration plot (Fig. 8, right panel) showed no deviations from the Henderson–Hasselbalch titration curve. This indicates that the observed deviation was caused by the multilamellar nature of the vesicles. This observation can be rationalized as follows. Fig. 8 (left panel) shows that at pH slightly below the probe pK_a the fraction of the non-protonated form of the nitroxide
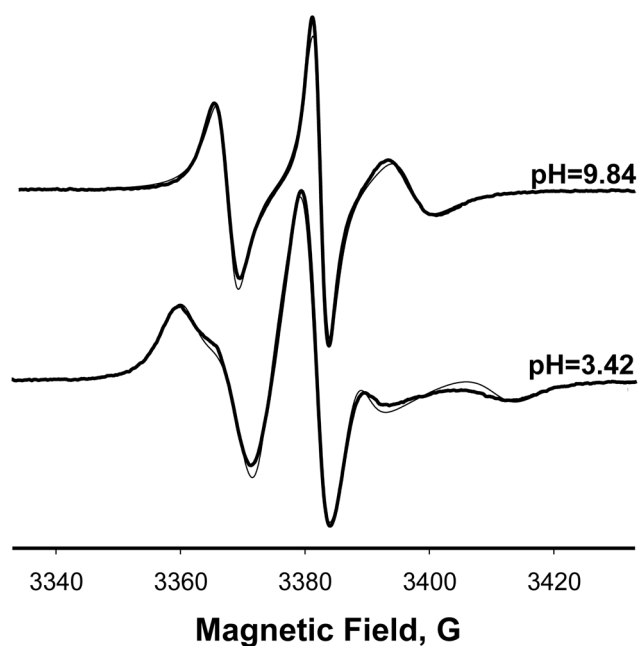

Fig. 5 Experimental (thick line) and least-squares simulated (thin) X-band EPR spectra of multilamellar POPG vesicles doped with **20-PTE** at 1 mol%. Experimental spectra were measured at 17 °C and pH = 9.84 (non-protonated form, top) and pH = 3.42 (fully protonated, bottom). The effective rotational correlation time increased from $\tau \approx 1.4$ ns for the non-protonated nitroxide to $\tau \approx 8.3$ ns for the protonated form.
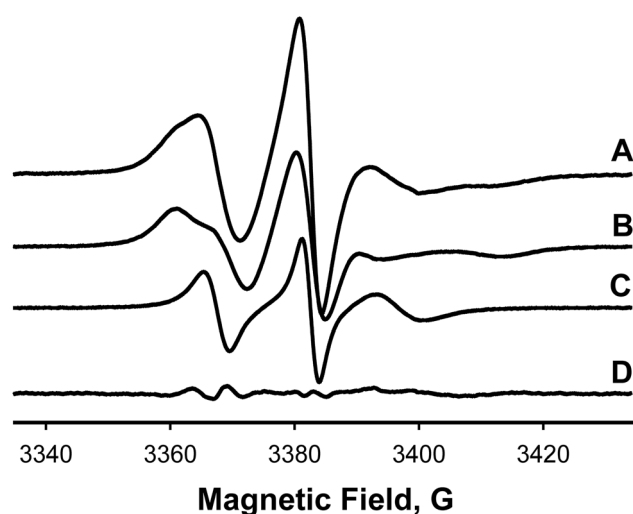

Fig. 6 Example of a least-squares decomposition of the experimental X-band EPR spectrum from multilamellar POPG vesicles doped with 1 mol% **20-PTE**. Spectrum was measured at 17 °C and pH = 6.97. (A) Experimental X-band EPR spectrum; (B) and (C) – least-squares simulated spectra of the protonated and non-protonated forms of the nitroxide, respectively; (D) residual of the fit – the difference between the experimental and simulated spectra.
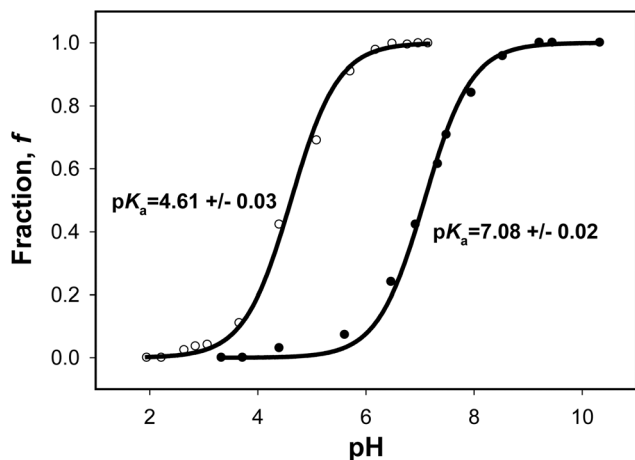
This journal is © The Royal Society of Chemistry 2024

Org. Biomol. Chem., 2024, **22**, 3652–3667 | **3659**

Fig. 7 Experimental EPR titration data for multilamellar POPC (○) and POPG (●) vesicles doped with spin-labelled lipid **22-PTE** at 1 mol%. Data were acquired at 17 °C. The fits to the Henderson−Hasselbalch equation are shown as solid lines and the best-fit pK_a values are indicated next to the plots.

Table 2 EPR titration data for spin-labelled lipids incorporated into multilamellar vesicles and measured at 17 °C

Spin-labeled lipid	ML vesicle lipid composition	pK_a	ΔpK_a[a]
22-PTE	POPC	4.61 ± 0.03	2.47 ± 0.04
22-PTE	POPG	7.08 ± 0.02	n/a
20-PTE	POPC	6.04 ± 0.06	1.63 ± 0.07
20-PTE	POPG	7.67 ± 0.04	n/a
23-DOPE	POPC	6.70 ± 0.05	1.53 ± 0.06
23-DOPE	POPG	8.23 ± 0.03	n/a

[a] ΔpK_a = pK_a(POPG) − pK_a(POPC).

ceased to follow the typical S-shaped titration curve, indicating that the fraction of the protonated form is accumulating slower than expected. In terms of the acid–base equilibrium, this means that there is a local factor that disfavours further positive charge development at the nitroxide moieties. One of such factors could be a positive charge of the choline quaternary ammonium groups from the leaflet of the adjacent lamella. The observed effect seems to be electrostatic in nature and comes into play when the amount of the positively charged nitroxide residues reaches a certain number (about 50% of the total amount in our case). We can safely assume that below this critical R˙H⁺ concentration the lipid system is capable of negating the electrostatic repulsion and accommodating these newly developed positive charges through conformational changes of phospholipid headgroups.[90,91] However, above this critical R˙H⁺ concentration, conformational changes in the headgroup region cannot negate the electrostatic repulsion any more, and further addition of acid results in formation of a smaller than expected fraction of the protonated nitroxides. Note that the upper half of the titration curve reaches plateau at pH ≈ pK_a + 2.0, which is typical for titration. The lower half, on the other hand, reaches the plateau at pH ≈ pK_a − 3.0, which is approximately one unit of pH lower than expected. Clearly, similar deviation from a single pK_a titration curve is not possible for the unilamellar vesicles, which have no adjacent lamellas. The answer to the question "why this effect was observed only for **20-PTE** but not **22-PTE** or **23-DOPE**" lies, most likely, in the structure and the length of the tether linking the nitroxide moiety to the phospholipid. We speculate that the observed phenomenon is a combination of the length and the conformational flexibility of the tether that makes the protonatable group readily affected by the charged choline residue. One way to check this hypothesis in the future will be to study MLVs containing a fraction of lipids with the
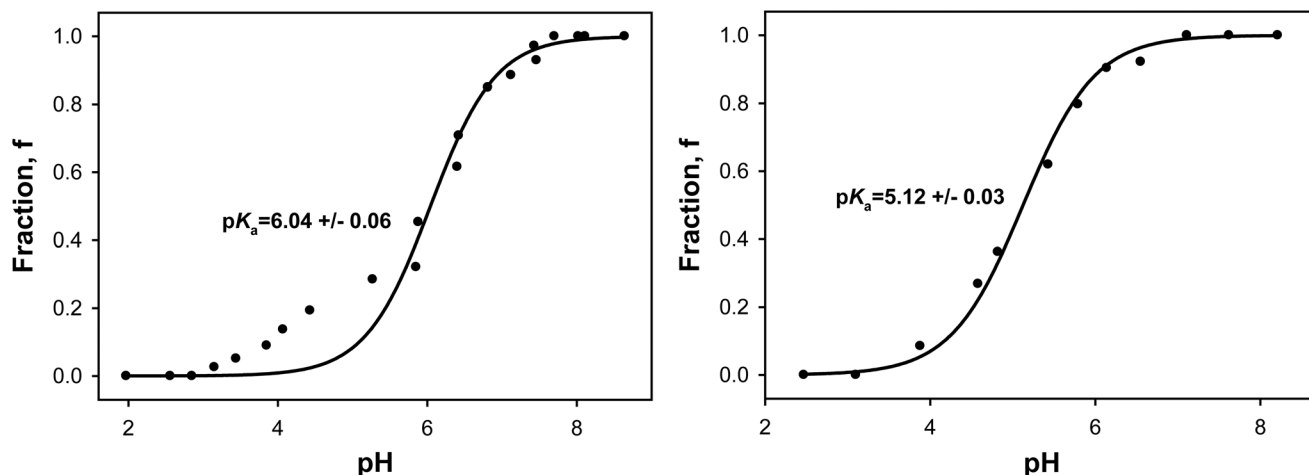

Fig. 8 Experimental EPR titration data for the spin-labeled lipid **20-PTE** in multilamellar (left) and 200 nm unilamellar (right) POPC vesicles. Data were acquired at 17 °C. The Henderson−Hasselbalch titration curves are shown as solid lines. Note that the experimental data in the left panel represent a combination of the data from two independent EPR titration experiments carried out over entire pH range.

3660 | *Org. Biomol. Chem.,* 2024, **22**, 3652–3667

This journal is © The Royal Society of Chemistry 2024

headgroups modified by PEG (polyethylene glycol) because PEG coatings of liposomes is known to shield the surface from aggregation.[92]

It should be noted here that the pK_a of **20-PTE** in 200 nm ULVs is significantly lower than MLVs prepared from the same lipids ($\Delta pK_a = 0.92 \pm 0.07$). Previously, we have observed a similar, but less sizable effect upon titration of another spin-labelled phospholipid, IKMTSL-PTE, in DMPG vesicles.[57] This effect was attributed to the difference in average packing density of lipids in the ULVs *vs.* MLVs that are composed of many lamellae of varying local curvatures. An interaction between adjacent lamellae could be another factor. Indeed, we have shown that the surface electrostatic potential of phosphatidylcholine MLVs such as those composed of DMPC is negative (*e.g.*, $\Psi \approx -100$ mV at 17 °C (ref. 56)). Then the presence of the adjacent lamellas in MLVs is expected to increase the negative surface potentials of the individual MLV bilayers *vs.* surface potential in ULVs and shift the observed local pK_a to higher values. However, further detailed investigation of this effect appears to be beyond the focus of the current study.

Conclusions

A concept for designing pH-sensitive nitroxides for studying electrostatic phenomena at biological interfaces based on changes in the shape of EPR spectra arising from a difference in molecular tumbling rates of the protonated and non-protonated forms, was demonstrated. Following this concept, a new series of protonatable nitroxide spin labels and probes of the pyrrolidine type was designed to exhibit a suitable range of pK_a values but not necessarily have a large effect of protonation on magnetic parameters of the nitroxide (*i.e.*, A_{iso}). The rotational motion of nitroxides at the biological interfaces, such as lipid bilayer surfaces, becomes significantly more restricted when these spin probes acquire an electric charge, and the fraction of such molecules can be readily derived by a straightforward decomposition of EPR spectra into two components. Since determination of the fractions of nitroxides in the charged-uncharged equilibria is based on the effects of molecular motion, such pH-sensitive probes may even show no measurable changes in magnetic parameters in order for the method described here to work.

The protonatable functionality in the newly synthesized nitroxides is not a part of the nitroxide heterocycle, as in pH-sensitive nitroxides of the 3-imidazoline and 1,3-imidazolidine series but is located in the side chain of the pyrrolidine nitroxide. These nitroxides demonstrated a rather small difference between the A_{iso} of the protonated and non-protonated forms, $\Delta A_{iso} \approx 0.50$ G, and the pK_a values varying within the range from $pK_a = 4.44 \pm 0.02$ to $pK_a = 6.73 \pm 0.01$. Click reaction between the new methanethiosulfonate spin labels and a head group thiol-modified phospholipid 1,2-dipalmitoyl-*sn*-glycero-3-phosphothioethanol (PTE) was employed for synthesizing the EPR-active pH-sensitive phospholipids. Yet another type of the EPR-active pH-sensitive phospholipid was synthesized *via*

one-step direct reductive amination of the ketone nitroxide with phosphatidylethanolamine lipid (DOPE). These new spin-labelled phospholipids report on their ionization state through the changes in the rotational dynamics. Indeed, the intermediate-to-slow-motion X-band EPR spectra of these spin-labelled phospholipids, doped to POPG or POPC MLVs at 1 mol%, demonstrated a gradual appearance of a more immobilized spectral component upon decrease in pH. The observed pH effect was attributed to the fact that the tumbling of the protonated nitroxide characterized by an effective rotational correlation time τ was significantly slowed down from $\tau \approx 1.4$ ns for uncharged nitroxide to $\tau \approx 8.3$ ns for the charge one due to the electrostatic interactions with the charged bilayer interface. The pK_a values of these new spin-labelled phospholipids were found to vary within a rather broad range from $pK_a = 4.61 \pm 0.03$ to $pK_a = 8.23 \pm 0.03$, depending on the structure of the protonatable head group and the composition of the lipid bilayer.

Overall, the feasibility of the concept of measuring local electrostatic phenomena at biological interfaces has been demonstrated. Spin-labelled phospholipids synthesized within the proposed approach were shown to exhibit rather pronounced pH-induced changes in EPR spectra characterized by protonation transitions with pK_a values varying within a rather broad pH range. The latter makes these phospholipids a valuable spectroscopic EPR probes for studying proton transfer-related and electrostatic phenomena in detergent micelles and at biological interfaces, such, for example, as lipid bilayer-water or lipid bilayer-membrane protein interface. We believe that the results of this proof-of-concept work will untie chemist's hands and open new avenues in designing the EPR active pH probes for biophysical studies.

Experimental section

Materials and methods

All chemicals and solvents were purchased from VWR International (Radnor, PA), Fisher Scientific (Waltham, MA), or Sigma-Aldrich (St Louis, MO), unless otherwise indicated, and used without additional purification. All solvents were reagent grade and used as received. 1,2-Dipalmitoyl-*sn*-glycero-3-phosphothioethanol (PTE), 1,2-dioleoyl-*sn*-glycero-3-phosphoethanolamine (DOPE), 1-palmitoyl-2-oleoyl-*sn*-glycero-3-phospho-(1′-*rac*-glycerol) (POPG), and 1-palmitoyl-2-oleoyl-*sn*-glycero-3-phosphocholine (POPC) were purchased from Avanti Polar Lipids (Alabaster, AL) as chloroform solutions (>99% pure) and used without further purification. 1-Oxyl-2,2,5,5-tetra-methyl-pyrrolidin-3-one **23** was a generous gift from Dr Igor A. Kirilyuk (Novosibirsk Institute of Organic Chemistry, Russia). Preparative thin layer chromatography was performed on a PTLC plate (Kieselgel 60 F254; Merck, Whitehouse, NJ). MS analysis was carried out using a high-resolution mass spectrometer Thermo Fisher Scientific Exactive™ Plus MS, a benchtop full-scan Orbitrap mass spectrometer, equipped with Heated Electrospray Ionization (HESI). Samples were introduced into the mass spectrometer *via* TriVersa NanoMate®

This journal is © The Royal Society of Chemistry 2024

Org. Biomol. Chem., 2024, **22**, 3652–3667 | **3661**

(Advion Interchim Scientific, Ithaca, NY). The mass spectrometer was operated in a positive ion mode. Infrared spectra were obtained with a Jasco FT/IR-4100 spectrometer (Jasco Inc., Easton, MD). ULVs were characterized by dynamic light scattering (DLS, Zetasizer, Malvern, Westborough, MA).

EPR measurements

X-band (9.5 GHz) continuous wave (CW) EPR spectra were recorded with a Varian (Palo Alto, CA) Century Series E-109 spectrometer interfaced to a PC. The sample temperature was maintained with stability better than ±0.02 °C and a gradient below 0.07 °C cm^{-1} over the sample region by a digital variable temperature accessory described previously.[93] Aqueous solutions or lipid suspensions were drawn into a poly(tetrafluoroethylene) capillary (i.d. = 0.81 mm, o.d. = 1.12 mm, NewAge Industries, Inc., Southampton, PA), and the capillary was folded and inserted into a i.d. = 3 mm, o.d. = 4 mm clear fused quartz EPR tube open from both ends (VWR International). Typical spectrometer settings were as follows: the modulation amplitude was set to a quarter or a half of the narrowest line peak-to-peak line width; time constant, 64 ms; incident microwave power, 2 mW; sweep time, 30 s; and scan width, 100 G. Typically, between 10 and 50 individual scans were acquired and averaged out.

EPR titration experiments

EPR titration experiments in aqueous solution were carried out in 50 mM phosphate buffer solutions adjusted to a required pH. In all the experiments the pH values were measured with a SimpHony pH meter (VWR International) equipped with InLab microcombination pH electrode (Mettler-Toledo GmbH, Greifensee, Switzerland) three-point calibrated using two sets of standard VWR (VWR International) buffer solutions: one at pH = 1.68, 4.0, and 7.0 and another at pH = 4.0, 7.0, and 10.0. Before the measurements, both the samples and the standard buffer solution were equilibrated at a required temperature using a circulating bath Model 9710 (PolyScience, Niles, IL) equipped with a digital temperature controller. For EPR titration and pH equilibration of MLVs, approximately 50–100 µl of lipid dispersion was placed into a 1.5 ml Eppendorf tube and the pH of the solution was adjusted by titration with a 0.3 or 0.05 M HCl solution or a 0.1 M NaOH solution. To ensure pH equilibration inside the MLVs after adjusting the pH, the dispersion was subjected to ten consecutive freeze–thaw cycles between liquid nitrogen and a water bath maintained at the temperature of the EPR experiment. The sample was vortexed occasionally, and the pH was measured at the temperature of the EPR experiment. For titration and pH equilibration of ULVs, the pH of the lipid dispersion was adjusted by titration with a 0.3 or 0.05 M HCl solution or a 0.1 M NaOH solution, and the sample was allowed to equilibrate for 10–15 min at the temperature of experiment with occasional vortexing.

Potentiometric titration

Potentiometric titration in aqueous solution was carried out at room temperature (21 °C) as follows. 3 mM solution of the

nitroxide 10 in DI water was acidified with HCl down to pH = 3.66 (completely protonated form of the nitroxide) and titrated with 10 mM NaOH solution. Experimental data and the fit are shown in Fig. S1 of the ESI.† The pH of the solution was measured with a SimpHony pH meter equipped with InLab microcombination pH electrode three-point calibrated using standard VWR buffer solutions at pH = 1.68, 4.0, and 7.0.

3-Cyano-2,2,5,5-tetramethyl-2,5-dihydro-1*H*-pyrrole 1-oxyl was synthesized according to the literature procedure.[66]

3-Amino-4-cyano-2,2,5,5-tetramethylpyrrolidine 1-oxyl.[67] Commercial ammonium hydroxide was cooled with ice-water bath to *ca.* 0 °C and saturated with dry gaseous NH$_3$. The concentration of the resulted NH$_3$ solution was estimated to be 44 w/v %. 3-Cyano-2,2,5,5-tetramethylpyrroline 1-oxyl (7.33 g, 44.4 mmol) was suspended in 25 ml of this NH$_3$ solution, the flack was sealed tight, and the reaction mixture was allowed to stay for 4 days upon stirring. After that, another 25 ml of concentrated NH$_3$ solution were added and stirring was continued for 4 days more. The reaction mixture was saturated with NaCl, and the precipitate formed (3-carbamido-2,2,5,5-tetramethyl-2,5-dihydro-1*H*-pyrrole 1-oxyl) was collected on a filter. Aqueous solution was extracted with ethyl acetate; organic extract was dried over MgSO$_4$ and concentrated under reduced pressure. A residue was treated with ether and precipitated another portion of 3-carbamido-2,2,5,5-tetramethyl-2,5-dihydro-1*H*-pyrrole 1-oxyl was collected on a filter. Overall, 1.93 g (23.8%) of amide was collected. Ether solution was concentrated and separated by chromatography on Al$_2$O$_3$, first with hexane–EtOAc, 50 : 50 (v/v), and then with hexane–EtOAc, 40 : 60 (v/v), as eluents, to give 3-amino-4-cyano-2,2,5,5-tetramethylpyrrolidine 1-oxyl (5.06 g, 62.6%). Also, 0.14 g (1.9%) of the starting nitrile was recovered.

3-Amino-1-oxyl-2,2,5,5-tetramethylpyrrolidine-4-carboxylic acid (POAC, 5).[67] A mixture of 3-amino-4-cyano-2,2,5,5-tetramethylpyrrolidine 1-oxyl (3.36 g, 18.5 mmol), Ba(OH)$_2$·8H$_2$O (22 g, 69.7 mmol), and water (125 ml) was refluxed for 48 h. After that, a solid phase was filtered off; an aqueous phase was diluted two-fold with water, and dry CO$_2$ was added portionwise, slowly. The precipitate formed was filtered off, and the aqueous solution was treated with dry CO$_2$ again. The CO$_2$ treatment followed by filtration was repeated until the solution stayed clear after CO$_2$ addition. Clear aqueous solution was lyophilized giving crude POAC (3.5 g, 97%), which was used without further purification.

3-*tert*-Butoxycarbonylamino-1-oxyl-2,2,5,5-tetramethylpyrrolidine-4-carboxylic acid (N-Boc POAC, 6). To a suspension of POAC 5 (4.16 g, 20.7 mmol) in 30 ml of dry acetonitrile, triethylamine (6.65 ml, 47.8 mmol) and di-*tert*-butyl dicarbonate (5.9 g, 27 mmol) were added consecutively upon stirring. The resulting mixture was stirred for 48 h at room temperature. After that, volatiles were removed under a reduced pressure, water (100 ml) was added to a residue, and pH of the aqueous phase was brought to pH ≈2.0 with 2N HCl. The aqueous phase was extracted with ethyl acetate and the organic extract was dried over Na$_2$SO$_4$. Ethyl acetate was removed under a reduced pressure; the resulting crude solids were triturated in chloro-

3662 | *Org. Biomol. Chem.*, 2024, **22**, 3652–3667

This journal is © The Royal Society of Chemistry 2024

form to give the target compound as a yellow precipitate, 2.9 g (46%). mp 204–208 °C (dec). FT-IR (KBr, λ_{max}, cm^{-1}): 3384, 3114 (br), 2987, 2939, 1743, 1686, 1523, 1368, 1298, 1279, 1170, 1143, 1045. HRMS-ESI: m/z calcd for $C_{14}H_{25}N_2O_5$ [M]$^+$ 301.17580, found 301.17569; calcd for $C_{14}H_{25}N_2O_5K$ [M + K]$^+$ 340.13951, found 340.13951.

3-*tert*-Butoxycarbonylamino-4-hydroxymethyl-1-oxyl-2,2,5,5-tetramethylpyrrolidine 8. Step 1. Triethylamine (0.52 ml, 3.7 mmol) was added to a suspension of *N*-Boc POAC 6 (1 g, 3.3 mmol) in dry ether (60 ml), and dry CH_2Cl_2 (40 ml) was added to make a clear solution. The resulting solution was cooled down to −10 °C, and a solution of ethyl chloroformate (0.35 ml, 3.7 mmol) in 5 ml of ether was added dropwise upon stirring. The reaction mixture was allowed to warm up to room temperature and stirring was continued for 3 h. After that, the reaction mixture was evaporated under a reduced pressure to dryness, the residue was dissolved in ether (25 ml), and a solution was filtered through a filter paper to give crude mixed anhydride 7.

Step 2. Sodium borohydride (1.25 g, 33 mmol) was added to EtOH (75 ml) cooled to −15 °C, and an ether solution of the mixed anhydride 7 from **Step 1** was added dropwise upon stirring and cooling. The reaction mixture was allowed to stay for 2 h (slowly warmed up to the room temperature). The reaction mixture was evaporated to dryness, water (20 ml) was added to the residue, and the mixture was extracted with chloroform. Organic extract was dried over Na_2SO_4. The product was purified on silica gel, with CHCl$_3$ containing 4.5 v/v% of CH$_3$OH as eluent to give 0.75 g of hydroxymethyl derivative 8 as a light yellow solid (79% yield after two steps). mp 196–198 °C (dec) (hexane–EtOAc). FT-IR (KBr, λ_{max}, cm^{-1}): 3339 (br), 3375 (br), 2985, 2970, 2934, 2877, 2813, 1686, 1518, 1362, 1301, 1288, 1167, 1052, 1004, 860, 755. HRMS-ESI: m/z calculated for $C_{14}H_{27}N_2O_4$ [M]$^+$ 287.19653, found 287.19621.

3-Amino-4-hydroxymethyl-1-oxyl-2,2,5,5-tetramethylpyrrolidine 9. N-Boc nitroxide 8 (0.761 g, 2.6 mmol) in a mixture of water (100 ml) and CH$_3$OH (15 ml) was refluxed[68] until TLC test (silica gel, CHCl$_3$ + CH$_3$OH) showed no presence of the starting compound (≈22 h). After that, the reaction mixture was saturated with solid KOH and extracted with chloroform (4 × 30 ml). Organic solution was extracted with 3% HCl (4 × 20 ml), acidic solution was washed with chloroform (2 × 20 ml), basified with solid KOH, and extracted with chloroform (4 × 20 ml). Organic extract was dried over Na_2SO_4. Evaporation of chloroform under a reduced pressure afforded 9 as a slightly yellow viscous oil (crystallized in 4 °C fridge) that was used without further purification. R_f = 0.4 (silica gel, CHCl$_3$ + 1.5% v/v CH$_3$OH). Yield 0.446 g (90%). mp 120–121 °C (hexane–EtOAc). FT-IR (KBr, λ_{max}, cm^{-1}): 3331, 3284, 3194, 2978, 2932, 2898, 2873, 1612, 1466, 1362, 1180, 1100, 1039, 986, 955, 941, 760. HRMS-ESI: m/z calcd for $C_9H_{20}N_2O_2$ [M + H]$^+$ 188.15193, found 188.15146.

3-Dimethylamino-4-hydroxymethyl-1-oxyl-2,2,5,5-tetramethylpyrrolidine 10. An amino derivative 9 (0.106 g, 0.57 mmol) was dissolved in 5 ml of 37% aqueous solution of formaldehyde, 130 μl of 88% formic acid was added, and the reaction mixture was heated and maintained at 60 °C upon stirring. In 2.5 h 130 μl of formic acid was added, and the heating was continued for 2 h. The course of reaction was controlled by TLC (silica gel, CHCl$_3$ + 1.5% v/v CH$_3$OH, compound 10 has R_f = 0.75). After the reaction was over, the reaction mixture was basified with 10% NaOH solution to pH≈10 and extracted with CHCl$_3$ (2 × 15 ml). Chloroform extract was dried over Na_2SO_4 and concentrated under a reduced pressure. After purification on silica gel (CHCl$_3$ + 1% v/v of CH$_3$OH) nitroxide 10 was obtained as a yellow solid, yield 0.105 g (86%). mp 127–129 °C (hexane–EtOAc). FT-IR (KBr, λ_{max}, cm^{-1}): 3398, 2973, 2932, 2922, 2893, 2828, 2791, 2778, 1478, 1449, 1359, 1308, 1207, 1177, 1133, 1088, 1042, 1032. HRMS-ESI: m/z calcd for $C_{11}H_{24}N_2O_2$ [M + H]$^+$ 216.18323, found 216.18314.

Methanesulfonic acid (4-dimethylamino-1-oxyl-2,2,5,5-tetramethyl-pyrrolidin-3-yl)methyl ester 11. A solution of dimethylamino nitroxide 10 (0.244 g, 1.1 mmol) and Et$_3$N (181 μl, 1.3 mmol) in dry CH_2Cl_2 (20 ml) was cooled down to −10 °C, and a solution of CH_3SO_2Cl (101 μl, 1.3 mmol) in 3 ml of CH_2Cl_2 was added dropwise upon stirring. In 5 min the cooling bath was removed and stirring continued at room temperature for 3 h. The reaction mixture was diluted with 10 ml of CH_2Cl_2, washed with water (3 × 10 ml), 5% solution of NaHCO$_3$ (2 × 10 ml), and dried over Na_2SO_4. After the solvent evaporation a light yellow solid of the methanesulfonyl derivative 11 was acquired, 0.316 g (95%). mp 96–98 °C (hexane–EtOAc). FT-IR (KBr, λ_{max}, cm^{-1}): 3023, 3007, 2974, 2930, 2875, 2833, 2786, 1477, 1456, 1351, 1172, 952, 844. HRMS-ESI: m/z calcd for $C_{12}H_{26}N_2O_4S$ [M + H]$^+$ 294.16078, found 294.16035.

3-Bromomethyl-4-dimethylamino-1-oxyl-2,2,5,5-tetramethyl-pyrrolidine 13. LiBr (87.8 mg, 1.01 mmol) was added to a solution of methanesulfonyl derivative 11 (35 mg, 0.119 mmol) in dry DMSO (4 ml) and heated at 70 °C for 10 h. The reaction mixture was diluted with a brine (15 ml), extracted with EtOAc, organic extract was thoroughly washed with brine (4 × 5 ml), dried over Na_2SO_4, and concentrated under reduced pressure; the residue was separated by preparative TLC (silica gel, hexane–EtOAc, 3 : 2 v/v, R_f = 0.69) to give 13 as a yellow crystalline solid, yield 73%, mp 90–92 °C (hexane–EtOAc). FT-IR (KBr, λ_{max}, cm^{-1}): 3026, 2988, 2973, 2932, 2922, 2871, 2837, 2794, 2786, 1481, 1470, 1449, 1359, 1281, 1253, 1223, 1175, 1077, 1061, 1044, 991, 962, 879, 648. HRMS-ESI: m/z calcd for $C_{11}H_{23}BrN_2O$ [M + H]$^+$ 278.09883 (^{79}Br) and 280.09733 (^{81}Br), found 278.09836 and 280.09573.

3-Dimethylamino-4-iodomethyl-1-oxyl-2,2,5,5-tetramethyl-pyrrolidine 14 was synthesized similar to 13. Organic extract was washed with 5% $Na_2S_2O_3$ solution, then with a brine. Chromatographic purification (silica gel, hexane–EtOAc, 3 : 2 v/v) afforded 14 as a light yellow powder, yield 33%, mp 99–102 °C (dec) (hexane). FT-IR (KBr, λ_{max}, cm^{-1}): 3026, 2970, 2932, 2917, 2871, 2837, 2799, 1481, 1372, 1359, 1212, 1186, 1173, 1071, 1055, 1039, 957, 877. HRMS-ESI: m/z calcd for $C_{11}H_{23}IN_2O$ [M + H]$^+$ 326.08496, found 326.08464.

3-Azidomethyl-4-dimethylamino-1-oxyl-2,2,5,5-tetramethyl-pyrrolidine 15 was synthesized similar to 13. Purification on

This journal is © The Royal Society of Chemistry 2024

Org. Biomol. Chem., 2024, **22**, 3652–3667 | **3663**

silica gel using hexane–EtOAc mixture (3 : 2 v/v) as an eluent (R_f = 0.49) gave **15** as a yellow solid, yield 93%. mp 48–50 °C (hexane–EtOAc). FT-IR (KBr, λ_{max}, cm^{-1}): 2979, 2969, 2933, 2833, 2794, 2781, 2098, 1481, 1451, 1370, 1358, 1283, 1243, 1225, 1174, 1074, 1038, 897, 817. HRMS-ESI: m/z calcd for $C_{11}H_{23}N_5O$ $[M + H]^+$ 241.18971, found 241.18917.

(2-Bromoethyl)carbamic acid (4-dimethylamino-1-oxyl-2,2,5,5-tetramethylpyrrolidin-3-yl)methyl ester 21. 2-Bromoethyl isocyanate (40 μl, 0.443 mmol) was added to a solution of the nitroxide **10** (45 mg, 0.209 mmol) in EtOAc (5 ml) and the reaction mixture was stirred at room temperature for 72 h (monitored by TLC, silica gel, CHCl$_3$ + 5% v/v CH$_3$OH as eluent). The reaction mixture was concentrated under a reduced pressure and the residue was purified on silica gel using CHCl$_3$ + 5% v/v CH$_3$OH as an eluent. The bromo-derivative **21** was obtained as a yellow solid, yield 68 mg (89%). mp 108–111 °C (hexane–EtOAc). FT-IR (KBr, λ_{max}, cm^{-1}): 3316, 3044, 2975, 2929, 2871, 2837, 2783, 1718, 1708, 1623, 1532, 1362, 1244, 1215, 1175, 1141, 1047, 965, 781, 656. HRMS-ESI: m/z calcd for $C_{14}H_{28}BrN_3O_3$ $[M + H]^+$ 365.13086 (^{79}Br) and 367.12936 (^{81}Br), found 365.13074 and 367.12814.

(2-((Methylsulfonyl)thio)ethyl)carbamic acid (4-(dimethyl-amino)-1-oxyl-2,2,5,5-tetramethyl-pyrrolidin-3-yl)methyl ester 22. Sodium methanethiosulfonate dihydrate NaSSO$_2$CH$_3$·2H$_2$O (71.7 mg, 0.422 mmol) was added to a solution of bromo derivative **21** (30.8 mg, 8.44 × 10^{-5} mol) in 1 ml of dry DMSO, and the reaction mixture was allowed to stay at room temperature. After the reaction was completed (monitored by TLC, silica gel, CHCl$_3$ + 5% v/v CH$_3$OH), the reaction mixture was diluted with a brine and extracted with EtOAc. An organic extract was thoroughly washed with brine, dried over Na$_2$SO$_4$, and concentrated under reduced pressure. After a separation on silica gel using CHCl$_3$ + 5% v/v CH$_3$OH as an eluent, the methanethiosulfonate **22** was obtained as a dark yellow viscous oil, 23 mg (70%). FT-IR (neat, λ_{max}, cm^{-1}): 3331, 2975, 2927, 2873, 2850, 2783, 1712, 1526, 1455, 1362, 1319, 1257, 1130, 1047, 957, 743. HRMS-ESI: m/z calcd for $C_{15}H_{31}N_3O_5S_2$ $[M + H]^+$ 397.16996, found 397.16975.

Synthesis of the adduct 16. A solution of 3-amino-1-(11,12-didehydrodibenzo[*b,f*]azocin-5(6*H*)-yl)propan-1-one (DBCO-amine) (0.0031 g, 1.125 × 10^{-5} mol) in 0.5 ml of acetonitrile was added to a solution of azide **15** (0.0027 g, 1.125 × 10^{-5} mol) in 0.5 ml of acetonitrile, and the resulting mixture was allowed to stay for 6 h. TLC analysis (silica gel deactivated with Et$_3$N, CHCl$_3$–CH$_3$OH–Et$_3$N (100 : 3 : 0.5 v/v) as an eluent) showed no presence of the starting materials. After a chromatographic purification, compound **16** was obtained as a crystalline solid, R_f = 0.31 (silica gel deactivated with Et$_3$N, CHCl$_3$–CH$_3$OH–Et$_3$N (100 : 3 : 0.5 v/v) as an eluent), yield 0.0057 g (98%). FT-IR (neat, λ_{max}, cm^{-1}): 3419, 2975, 2925, 1649, 1457, 1380, 1199, 1002, 967, 938, 781. HRMS-ESI: m/z calcd for $C_{29}H_{39}N_7O_2$ $[M + H]^+$ 517.31597, found 517.31558; m/z calcd for $C_{29}H_{40}N_7O_2$ $[M + 2H]^{2+}$ 259.16163, found 259.16149.

3-Dimethylamino-1-oxyl-2,2,5,5-tetramethyl-4-[2-(tetrahydro-pyran-2-yloxy)-ethoxymethyl]-pyrrolidine 17. 2-(2-Bromoethoxy)tetrahydro-2H-pyran (0.512 ml, 3.39 mmol) was added to a solution of the nitroxide **10** (182 mg, 0.847 mmol) in 12 ml DMSO containing crushed KOH (892 mg, 15.93 mmol). The reaction mixture was vigorously stirred at room temperature for 24 h. After that, inorganic precipitate was filtered off; DMSO solution was diluted with a brine (50 ml) and the resulting aqueous solution was extracted with EtOAc. The tetrahydropyran-protected nitroxide **17** was obtained as yellow viscous oil, 265 mg (91%). FT-IR (neat, λ_{max}, cm^{-1}): 2968, 2933, 2868, 2831, 2779, 1455, 1356, 1123, 1073, 1034, 867, 817. HRMS-ESI: m/z calcd for $C_{18}H_{36}N_2O_4$ $[M + H]^+$ 344.26696, found 344.26750.

3-Dimethylamino-4-(2-hydroxy-ethoxymethyl)-1-oxyl-2,2,5,5-tetramethylpyrrolidine 18. Deprotection of the nitroxide **17** was carried out similar to the literature procedure.[71] A solution of the O-THP derivative **17** (0.140 g, 0.408 mmol) in 3 ml of CH$_3$COOH–H$_2$O mixture (4 : 1 v/v) was heated at 50–55 °C for 3 h (monitored by TLC, silica gel, CHCl$_3$ + 1.5% v/v CH$_3$OH). After the reaction was completed, the reaction mixture was added dropwise upon vigorous stirring to a saturated NaHCO$_3$ solution (10 ml), after that solid NaOH was added to bring the pH up to pH = 10–11. The basic solution was extracted with EtOAc, organic extract was washed with brine, and dried over Na$_2$SO$_4$. After concentration under a reduced pressure the residue was purified on silica gel with CHCl$_3$ + 2% v/v CH$_3$OH as an eluent to give **18** as a yellow oil, yield 100 mg (94%). FT-IR (neat, λ_{max}, cm^{-1}): 3414, 2973, 2929, 2873, 2786, 1732, 1646, 1455, 1380, 1359, 1281, 1244, 1212, 1180, 1124, 1074, 1055, 1039. HRMS-ESI: m/z calcd for $C_{13}H_{28}N_2O_3$ $[M + H]^+$ 260.20944, found 260.20984.

2-((4-(Dimethylamino)-1-oxyl-2,2,5,5-tetramethylpyrrolidin-3-yl)methoxy)ethyl methanesulfonate 19. A solution of nitroxide **18** (46.4 mg, 0.179 mmol) and Et$_3$N (27.4 μl, 0.197 mmol) in 3 ml of dry CH$_2$Cl$_2$ was cooled down to −10 °C, and a solution of CH$_3$SO$_2$Cl (15.3 μl, 0.197 mmol) in 1 ml of CH$_2$Cl$_2$ was added dropwise upon stirring. In 5 min the cooling bath was removed, and the stirring continued at room temperature for 3 h. The reaction mixture was diluted with 5 ml of CH$_2$Cl$_2$, washed with water (2 × 5 ml), 5% solution of NaHCO$_3$ (1 × 5 ml), and dried over Na$_2$SO$_4$. Solvent evaporation afforded the methanesulfonyl derivative **19** as a yellow solid (57 mg, 94%). mp 78–80 °C (hexane–EtOAc). The compound was used without further purification. FT-IR (neat, λ_{max}, cm^{-1}): 2973, 2921, 2870, 2848, 2784, 1458, 1353, 1171, 1128, 1016, 969, 924, 807. HRMS-ESI: m/z calcd for $C_{14}H_{30}N_2O_5S$ $[M + H]^+$ 338.18699, found 338.18734.

S-(2-((4-(Dimethylamino)-1-oxyl-2,2,5,5-tetramethylpyrrolidin-3-yl)methoxy)ethyl) methanesulfonothioate 20. A DMSO solution (3 ml) containing methanesulfonyl nitroxide **19** (0.05 g, 0.148 mmol), NaSSO$_2$CH$_3$·2H$_2$O (0.1 g, 0.588 mmol), and LiBr (0.005 g, 5.76 × 10^{-5} mol) was heated at 70 °C for 40 min. The reaction mixture was diluted with a brine, extracted with EtOAc; an organic extract was washed with brine, dried over Na$_2$SO$_4$, and concentrated under a reduced pressure. After a separation on silica gel with CHCl$_3$ + 5% v/v CH$_3$OH as eluent, the methanethiosulfonate **20** was obtained as a yellow viscous

3664 | *Org. Biomol. Chem.*, 2024, **22**, 3652–3667

This journal is © The Royal Society of Chemistry 2024

oil, 0.012 g, yield 23%. FT-IR (neat, λ_{max}, cm^{-1}): 3005, 2986, 2976, 2935, 2903, 2882, 2830, 2800, 2775, 1475, 1454, 1356, 1313, 1210, 1134, 1118, 967, 745. HRMS-ESI: m/z calcd for $C_{14}H_{30}N_2O_4S_2$ [M + H]$^+$ 354.16415, found 354.16460.

Spin-labeling of 1,2-dipalmitoyl-*sn*-glycero-3-phosphothioethanol (PTE) (General procedure). 50 mM phosphate buffer pH = 6.86 (1.5 ml) was added to a chloroform solution (3 ml) containing 1,2-dipalmitoyl-*sn*-glycero-3-phosphothioethanol (sodium salt) (1.75×10^{-5} mol) and a methanethiosulfonate spin label (either **22** or **20**, 1.77×10^{-5} mol) and the resulting two-phase mixture was vigorously stirred for 24 h. Organic layer was separated, concentrated under a reduced pressure, and the residue was separated on silica gel. Spin-labeled phospholipids were obtained as yellowish viscous oils. **22-PTE**: a mixture CHCl$_3$–CH$_3$OH–H$_2$O (70 : 30 : 1 v/v) was used as an eluent, 70% yield. FT-IR (neat, λ_{max}, cm^{-1}): 3342, 2954, 2920, 2849, 1739, 1726, 1531, 1467, 1242, 1178, 1103, 1071, 1023. HRMS-ESI: m/z calcd for $C_{51}H_{99}N_3NaO_{11}PS_2$ [M + H]$^+$ 1047.63508, found 1047.63213. **20-PTE**: a mixture CHCl$_3$–CH$_3$OH–H$_2$O (70 : 15 : 0.5 v/v) was used as an eluent, 44% yield. FT-IR (neat, λ_{max}, cm^{-1}): 2949, 2917, 2847, 2793, 1742, 1464, 1376, 1362, 1239, 1167, 1097, 1068, 1017. HRMS-ESI: m/z calcd for $C_{50}H_{98}O_{10}N_2NaPS_2$ [M + H]$^+$ 1004.62927, found 1004.62864; $C_{50}H_{97}O_{10}N_2Na_2PS_2$ [M + Na]$^+$ 1026.61122, found 1026.61118.

Spin-labelling of 1,2-dioleoyl-*sn-glycero*-3-phosphoethanolamine (DOPE). 1-Oxyl-2,2,5,5-tetramethylpyrrolidin-3-one **23** (0.013 g, 8.33×10^{-5} mol) and 1,2-dioleoyl-*sn*-glycero-3-phosphoethanolamine (20 mg, 2.68×10^{-5} mol, 1 ml of chloroform solution) were mixed, diluted with 2 ml of CHCl$_3$ and 4 ml of i-PrOH, and tetrabutylammonium cyanoborohydride (0.023 g, 8.16×10^{-5} mol) was added upon stirring. The reaction mixture was heated at a slight reflux for 24 h (monitored by TLC). After concentration at a reduced pressure, the residue was separated on silica gel using a mixture CHCl$_3$–CH$_3$OH–H$_2$O (70 : 15 : 0.5 v/v) as an eluent affording **23-DOPE** as slightly yellow viscous oil. Yield 21.6 mg (91%). FT-IR (neat, λ_{max}, cm^{-1}): 3409, 2925, 2852, 1737, 1460, 1231, 1065, 821. HRMS-ESI: m/z calcd for $C_{49}H_{93}N_2O_9P$ [M + H]$^+$ 884.66132, found 884.59905.

Synthesis of mercaptoethanol adducts 24 and 25 was carried out similar to the previously described procedure.[55]

(2-((2-Hydroxyethyl)-disulfaneyl)ethyl)carbamic acid (4-(dimethylamino)-1-oxyl-2,2,5,5-tetramethylpyrrolidin-3-yl)methyl ester 24. Purified on silica gel with CHCl$_3$ + 5% v/v CH$_3$OH, the adduct **24** was obtained as a yellow viscous oil, yield 95%. FT-IR (neat, λ_{max}, cm^{-1}): 3326, 3063, 2973, 2930, 2871, 2786, 1705, 1531, 1459, 1362, 1255, 1178, 1141, 1044, 774. HRMS-ESI: m/z calcd for $C_{16}H_{33}N_3O_4S_2$ [M + H]$^+$ 395.19070, found 395.19043.

3-(Dimethylamino)-4-((2-((2-hydroxyethyl)disulfaneyl)-ethoxy)methyl)-2,2,5,5-tetramethyl-pyrrolidin-1-oxyl 25. Purified on silica gel with CHCl$_3$ + 5% v/v CH$_3$OH, the adduct **25** was obtained as a yellow viscous oil, yield 80%. FT-IR (neat, λ_{max}, cm^{-1}): 3401, 2979, 2925, 2866, 2783, 1459, 1387, 1357, 1282, 1242, 1210, 1178, 1117, 1076, 1044, 1010, 972. HRMS-ESI: m/z calcd for $C_{15}H_{32}N_2O_3S_2$ [M + H]$^+$ 352.18489, found 352.18531.

3-(2-Hydroxyethylamino)-1-oxyl-2,2,5,5-tetramethylpyrrolidine 26. An isopropanol solution (2 ml) containing H$_3$PO$_3$ (0.0115 g, 0.14 mmol) and ethanolamine (0.0085 g, 0.14 mmol) was prepared. The resulting solution was mixed with 23 (0.0044 g, 2.8×10^{-5} mol) dissolved in 1 ml of i-PrOH, and then NaCNBH$_3$ (0.0395 g, 0.14 mmol) was added. The reaction mixture was heated overnight (hot plate was set to 80 °C) upon stirring. Volatiles were removed under a reduced pressure, the residue was dissolved in CHCl$_3$; the organic layer was thoroughly washed with 5% solution of NaHCO$_3$, and dried over Na$_2$SO$_4$ to give 26 as a yellow oily product, 0.0029 g (51%). FT-IR (neat, λ_{max}, cm^{-1}): 3396, 2970, 2927, 2869, 2850, 1646, 1564, 1463, 1412, 1367, 1255, 1130, 1058, 967. HRMS-ESI: m/z calcd for $C_{10}H_{22}N_2O_2$ [M + H]$^+$ 202.16758, found 202.16735.

Author contributions

Conflicts of interest

There are no conflicts to declare.

Acknowledgements

References

1 A. Carrington and I. C. P. Smith, *Mol. Phys.*, 1964, **8**, 101–105.

2 H. Fischer, *Mol. Phys.*, 1965, **9**, 149–152.

3 H. Zeldes and R. Livingston, *J. Chem. Phys.*, 1966, **45**, 1946–1954.

4 H. Hogeveen, H. R. Gersmann and A. P. Praat, *Recl. Trav. Chim. Pays-Bas*, 1967, **86**, 1063–1065.

5 B. M. Hoffman and T. B. Eames, *J. Am. Chem. Soc.*, 1969, **91**, 2169–2170.

This journal is © The Royal Society of Chemistry 2024

Org. Biomol. Chem., 2024, **22**, 3652–3667 | **3665**

6   V. Malatesta and K. U. Ingold, *J. Am. Chem. Soc.*, 1973, **95**, 6404–6407.

7   V. A. Golubev, E. G. Rozantsev and M. B. Neiman, *Bull. Acad. Sci. USSR, Div. Chem. Sci.*, 1965, **14**, 1898–1904.

8   J. H. Osiecki and E. F. Ullman, *J. Am. Chem. Soc.*, 1968, **90**, 1078–1079.

9   D. S. Cafiso and W. L. Hubbell, *Biochemistry*, 1978, **17**, 3871–3877.

10 A. T. Quintanilha and R. J. Mehlhorn, *FEBS Lett.*, 1978, **91**, 104–108.

11 V. V. Khramtsov and L. B. Volodarsky, in *Biological Magnetic Resonance: Volume 14: Spin Labeling*, ed. L. J. Berliner, Springer US, Boston, MA, 2002, pp. 109–180.

12 E. F. Ullman, L. Call and J. H. Osiecki, *J. Org. Chem.*, 1970, **35**, 3623–3631.

13 J. F. W. Keana, M. J. Acarregui and S. L. M. Boyle, *J. Am. Chem. Soc.*, 1982, **104**, 827–830.

14 V. V. Khramtsov, L. M. Weiner, I. A. Grigoriev and L. B. Volodarsky, *Chem. Phys. Lett.*, 1982, **91**, 69–72.

15 T. I. V. Smirnova, M. A. Voinov and A. I. Smirnov, in *Encyclopedia of Analytical Chemistry: Applications, Theory, and Instrumentation*, ed. R. A. Meyers, John Wiley & Sons Inc., 2009.

16 M. A. Voinov and A. I. Smirnov, *Electron Paramagn. Reson.*, 2011, **22**, 71–106.

17 M. A. Voinov and A. I. Smirnov, *Methods Enzymol.*, 2015, **564**, 191–217.

18 W. Aoi and Y. Marunaka, *BioMed Res. Int.*, 2014, **2014**, 598986.

19 A. Sotgiu, K. Mäder, G. Placidi, S. Colacicchi, C. L. Ursini and M. Alecci, *Phys. Med. Biol.*, 1998, **43**, 1921–1930.

20 V. Khramtsov, I. Grigor'ev, M. Foster, D. Lurie and I. Nicholson, *Cell. Mol. Biol.*, 2000, **46**, 1361–1374.

21 A. N. Tikhonov, R. V. Agafonov, I. A. Grigor'ev, I. A. Kirilyuk, V. V. Ptushenko and B. V. Trubitsin, *Biochim. Biophys. Acta, Bioenerg.*, 2008, **1777**, 285–294.

22 V. V. Khramtsov, *Curr. Org. Chem.*, 2005, **9**, 909–923.

23 S. Koda, J. Goodwin, V. V. Khramtsov, H. Fujii and H. Hirata, *Anal. Chem.*, 2012, **84**, 3833–3837.

24 V. V. Khramtsov, I. A. Grigor'ev, M. A. Foster and D. J. Lurie, *Antioxid. Redox Signaling*, 2004, **6**, 667–676.

25 V. V. Khramtsov, G. L. Caia, K. Shet, E. Kesselring, S. Petryakov, J. L. Zweier and A. Samouilov, *J. Magn. Reson.*, 2010, **202**, 267–273.

26 D. I. Potapenko, M. A. Foster, D. J. Lurie, I. A. Kirilyuk, J. M. S. Hutchison, I. A. Grigor'ev, E. G. Bagryanskaya and V. V. Khramtsov, *J. Magn. Reson.*, 2006, **182**, 1–11.

27 M. A. Foster, I. A. Grigor'ev, D. J. Lurie, V. V. Khramtsov, S. McCallum, I. Panagiotelis, J. M. Hutchison, A. Koptioug and I. Nicholson, *Magn. Reson. Med.*, 2003, **49**, 558–567.

28 B. Gallez, K. Mäder and H. M. Swartz, *Magn. Reson. Med.*, 1996, **36**, 694–697.

29 A. Samouilov, O. V. Efimova, A. A. Bobko, Z. Sun, S. Petryakov, T. D. Eubank, D. G. Trofimov, I. A. Kirilyuk, I. A. Grigor'ev, W. Takahashi, J. L. Zweier and V. V. Khramtsov, *Anal. Chem.*, 2014, **86**, 1045–1052.

30 D. A. Komarov, I. Dhimitruka, I. A. Kirilyuk, D. G. Trofimov, I. A. Grigor'ev, J. L. Zweier and V. V. Khramtsov, *Magn. Reson. Med.*, 2012, **68**, 649–655.

31 V. V. Ptushenko, L. N. Ikryannikova, I. A. Grigor'ev, I. A. Kirilyuk, B. V. Trubitsin and A. N. Tikhonov, *Appl. Magn. Reson.*, 2006, **30**, 329–343.

32 D. A. Komarov, Y. Ichikawa, K. Yamamoto, N. J. Stewart, S. Matsumoto, H. Yasui, I. A. Kirilyuk, V. V. Khramtsov, O. Inanami and H. Hirata, *Anal. Chem.*, 2018, **90**, 13938–13945.

33 R. Nakaoka, K. Kato, K. Yamamoto, H. Yasui, S. Matsumoto, I. A. Kirilyuk, V. V. Khramtsov, O. Inanami and H. Hirata, *Anal. Chem.*, 2023, 3940–3950.

34 Y. Liu, F. A. Villamena and J. L. Zweier, *Chem. Commun.*, 2008, 4336–4338.

35 A. A. Bobko, I. Dhimitruka, J. L. Zweier and V. V. Khramtsov, *J. Am. Chem. Soc.*, 2007, **129**, 7240–7241.

36 I. Dhimitruka, A. A. Bobko, C. M. Hadad, J. L. Zweier and V. V. Khramtsov, *J. Am. Chem. Soc.*, 2008, **130**, 10780–10787.

37 A. A. Bobko, I. Dhimitruka, D. A. Komarov and V. V. Khramtsov, *Anal. Chem.*, 2012, **84**, 6054–6060.

38 E. G. Kovaleva, L. S. Molochnikov, D. O. Antonov, D. P. T. Stepanova, M. Hartmann, A. N. Tsmokalyuk, A. Marek and A. I. Smirnov, *J. Phys. Chem. C*, 2018, **122**, 20527–20538.

39 D. O. Antonov, D. P. Tambasova, A. B. Shishmakov, I. A. Kirilyuk and E. G. Kovaleva, *Gels*, 2021, **7**, 119.

40 E. G. Kovaleva, L. S. Molochnikov, E. L. Golovkina, M. Hartmann, I. A. Kirilyuk and I. A. Grigoriev, *Microporous Mesoporous Mater.*, 2015, **203**, 1–7.

41 E. G. Kovaleva, L. S. Molochnikov, D. Tambasova, A. Marek, M. Chestnut, V. A. Osipova, D. O. Antonov, I. A. Kirilyuk and A. I. Smirnov, *J. Membr. Sci.*, 2020, **604**, 118084.

42 V. Perelygin, M. A. Voinov, A. Marek, E. Ou, J. Krim, D. Brenner, T. I. Smirnova and A. I. Smirnov, *J. Phys. Chem. C*, 2019, **123**, 29972–29985.

43 M. Edeleva, G. Audran, S. Marque and E. Bagryanskaya, *Materials*, 2019, **12**, 688.

44 Y. Le Du, L. Binet, P. Hémery and L. Marx, *J. Polym. Sci., Part A: Polym. Chem.*, 2012, **50**, 2871–2877.

45 M. V. Edeleva, I. A. Kirilyuk, I. F. Zhurko, D. A. Parkhomenko, Y. P. Tsentalovich and E. G. Bagryanskaya, *J. Org. Chem.*, 2011, **76**, 5558–5573.

46 D. A. Parkhomenko, M. V. Edeleva, V. G. Kiselev and E. G. Bagryanskaya, *J. Phys. Chem. B*, 2014, **118**, 5542–5550.

47 G. Gryn'ova, L. M. Smith and M. L. Coote, *Phys. Chem. Chem. Phys.*, 2017, **19**, 22678–22683.

48 A. I. Smirnov and R. L. Belford, *J. Magn. Reson., Ser. A*, 1995, **113**, 65–73.

49 T. I. Smirnova, A. I. Smirnov, R. B. Clarkson and R. L. Bedford, *J. Phys. Chem.*, 1995, **99**, 9008–9016.

50 A. I. Smirnov, T. I. Smirnova and P. D. Morse, *Biophys. J.*, 1995, **68**, 2350–2360.

51 A. I. Smirnov and T. I. Smirnova, in *EPR: Instrumental Methods*, ed. L. J. Berliner and C. J. Bender, Springer US, Boston, MA, 2004, pp. 277–348.

3666 | *Org. Biomol. Chem.*, 2024, **22**, 3652–3667

This journal is © The Royal Society of Chemistry 2024

52 M. A. Voinov, J. F. Polienko, T. Schanding, A. A. Bobko, V. V. Khramtsov, Y. V. Gatilov, T. V. Rybalova, A. I. Smirnov and I. A. Grigor'ev, *J. Org. Chem.*, 2005, **70**, 9702–9711.

53 K. Margita, M. A. Voinov and A. I. Smirnov, *Cell Biochem. Biophys.*, 2017, **75**, 185–193.

54 V. V. Khramtsov, L. M. Weiner, S. I. Eremenko, O. I. Belchenko, P. V. Schastnev, I. A. Grigorev and V. A. Reznikov, *J. Magn. Reson.*, 1985, **61**, 397–408.

55 M. A. Voinov, I. A. Kirilyuk and A. I. Smirnov, *J. Phys. Chem. B*, 2009, **113**, 3453–3460.

56 M. A. Voinov, I. Rivera-Rivera and A. I. Smirnov, *Biophys. J.*, 2013, **104**, 106–116.

57 M. A. Voinov, C. T. Scheid, I. A. Kirilyuk, D. G. Trofimov and A. I. Smirnov, *J. Phys. Chem. B*, 2017, **121**, 2443–2453.

58 M. D. Barratt and P. Laggner, *Biochim. Biophys. Acta, Biomembr.*, 1974, **363**, 127–133.

59 M. Egretcharlier, A. Sanson, M. Ptak and O. Bouloussa, *FEBS Lett.*, 1978, **89**, 313–316.

60 L. I. Horvath, P. J. Brophy and D. Marsh, *Biochemistry*, 1988, **27**, 5296–5304.

61 M. Esmann and D. Marsh, *Biochemistry*, 1985, **24**, 3572–3578.

62 D. S. Cafiso and W. L. Hubbell, *Annu. Rev. Biophys. Bioeng.*, 1981, **10**, 217–244.

63 M. J. Stephen, *J. Chem. Phys.*, 1971, **55**, 3878–3883.

64 C. S. Klug and J. B. Feix, in *Methods in Cell Biology*, Academic Press, 2008, vol. 84, pp. 617–658.

65 M. A. Voinov, A. Ruuge, V. A. Reznikov, I. A. Grigor'ev and A. I. Smirnov, *Biochemistry*, 2008, **47**, 5626–5637.

66 E. G. Rozantzev and L. A. Krinitzkaya, *Tetrahedron*, 1965, **21**, 491–497.

67 A. Rassat and P. Rey, *Bull. Soc. Chim. Fr.*, 1967, 815–818.

68 C. Zinelaabidine, O. Souad, J. Zoubir, B. Malika and A. Nour-Eddine, *Int. J. Chem.*, 2012, **4**, 73.

69 C. G. Gordon, J. L. Mackey, J. C. Jewett, E. M. Sletten, K. N. Houk and C. R. Bertozzi, *J. Am. Chem. Soc.*, 2012, **134**, 9199–9208.

70 A. V. Strizhak, K. Sharma, O. Babii, S. Afonin, A. S. Ulrich, I. V. Komarov and D. R. Spring, *Org. Biomol. Chem.*, 2018, **16**, 8559–8564.

71 D. R. Williams and W. S. Kissel, *J. Am. Chem. Soc.*, 1998, **120**, 11198–11199.

72 L. A. Krinitskaya, E. G. Rozantsev and M. B. Neiman, *Bull. Acad. Sci. USSR, Div. Chem. Sci.*, 1965, **14**, 100–102.

73 N. S. Zefirov, N. V. Zyk, E. K. Beloglazkina and A. G. Kutateladze, *Sulfur Rep.*, 1993, **14**, 223–240.

74 H. Y. Yoon, D. Lee, D. K. Lim, H. Koo and K. Kim, *Adv. Mater.*, 2022, **34**, 28.

75 M. F. Debets, S. S. van Berkel, J. Dommerholt, A. J. Dirks, F. P. J. T. Rutjes and F. L. van Delft, *Acc. Chem. Res.*, 2011, **44**, 805–815.

76 E. M. Sletten and C. R. Bertozzi, *Acc. Chem. Res.*, 2011, **44**, 666–676.

77 V. V. Khramtsov, L. M. Weiner, S. I. Eremenko, O. I. Belchenko, P. V. Schastnev, I. A. Grigor'ev and V. A. Reznikov, *J. Magn. Reson.*, 1985, **61**, 397–408.

78 V. V. Khramtsov and L. M. Weiner, *Russ. Chem. Rev.*, 2007, **57**, 824–838.

79 Chemical Book, CAS DataBase List **https://www.chemicalbook.com/ChemicalProductProperty_EN_CB32730210.htm**.

80 J. Catalan, J. L. M. Abboud and J. Elguero, *Adv. Heterocycl. Chem.*, 1987, **41**, 187–274.

81 A. Albert and P. J. Taylor, *J. Chem. Soc., Perkin Trans. 2*, 1989, 1903–1905.

82 J. L. M. Abboud, C. Foces-Foces, R. Notario, R. E. Trifonov, A. P. Volovodenko, V. A. Ostrovskii, I. Alkorta and J. Elguero, *Eur. J. Org. Chem.*, 2001, **2001**, 3013–3024.

83 S. Stoll and A. Schweiger, *J. Magn. Reson.*, 2006, **178**, 42–55.

84 S. Stoll, easyspin, easyspin.org.

85 EasySpin Academy, **https://www.youtube.com/watch?v=uy_smGyxZxc&t=26s**.

86 A. I. Smirnov, R. Belford and R. Clarkson, in *Spin Labeling: The Next Millennium*, ed. L. J. Berliner, Plenum Press, New York, 2002, vol. 16, ch. 3, pp. 83–107.

87 A. F. Gulla and D. E. Budil, *J. Phys. Chem. B*, 2001, **105**, 8056–8063.

88 T. I. Smirnova and A. I. Smirnov, in *ESR Spectroscopy in Membrane Biophysics*, ed. M. A. Hemminga and L. J. Berliner, Springer US, New York, 2007, vol. 27, ch. 6, pp. 165–251.

89 D. Marsh, *Handbook of Lipid Bilayers*, CRC Press, 2nd edn, 2013, DOI: **10.1201/b11712**.

90 M. Roux, J. M. Neumann, R. S. Hodges, P. F. Devaux and M. Bloom, *Biochemistry*, 1989, **28**, 2313–2321.

91 J. P. F. Doux, B. A. Hall and J. A. Killian, *Biophys. J.*, 2012, **103**, 1245–1253.

92 J. S. Suk, Q. Xu, N. Kim, J. Hanes and L. M. Ensign, *Adv. Drug Delivery Rev.*, 2016, **99**, 28–51.

93 A. M. Alaouie and A. I. Smirnov, *J. Magn. Reson.*, 2006, **182**, 229–238.

This journal is © The Royal Society of Chemistry 2024

Org. Biomol. Chem., 2024, **22**, 3652–3667 | **3667**